A THEORETICAL MODEL ANALYSIS OF ABSORPTION OF A THREE LEVEL DIODE PUMPED ALKALI LASER

THESIS

Charlton D. Lewis, II, 1st Lt, USAF

AFIT/GAP/ENP/09-M07

DEPARTMENT OF THE AIR FORCE
AIR UNIVERSITY

AIR FORCE INSTITUTE OF TECHNOLOGY

Wright-Patterson Air Force Base, Ohio

AFIT/GAP/ENP/09-M07

A THEORETICAL MODEL ANALYSIS OF ABSORPTION OF A THREE LEVEL DIODE PUMPED ALKALI LASER

THESIS

Presented to the Faculty

Department of Engineering Physics

Graduate School of Engineering and Management

Air Force Institute of Technology

Air University

Air Education and Training Command

In Partial Fulfillment of the Requirements for the

Degree of Master of Science in Applied Physics

Charlton D. Lewis, II, BS

1st Lt, USAF

March 2009

AFIT/GAP/ENP/09-M07

A THEORETICAL MODEL ANALYSIS OF ABSORPTION OF A THREE LEVEL DIODE PUMPED ALKALI LASER

Charlton D. Lewis, II, BS

1st Lt, USAF

Approved:

Glen P. Perram, PhD (Chairman)	17 MAR 09 Date
William F. Bailey, PhD (Member)	17 Mar 2009 Date
Lt Col Jeremy C. Holtgrave, PhD (Member)	18 Mar 2009 Date

Abstract

This paper models the absorption phenomena of light in a three level diode pumped alkali laser system. Specifically this model calculates for a user defined set of system parameters the attenuation of the input pump beam and characteristics of the bleached wave. Using Wolfram's Mathematica 6.0 software all necessary physics for an accurate description of absorption was modeled from first principles: energy levels, cross sections, spin-orbit kinetic processes, saturation frequencies, pump attenuation, and differential transmittance, which is a representation of the bleached wave. A specific DPAL scenario was simulated, 455K system temperature, alkali concentration of $6.1 \cdot 10^{13}$, and a system pressure of 200 torr of He and 600 torr of Ethane. For a range of initial input intensities the linear approximation to the beam attenuation predicted consistently a differential transmittance value of 70%. It was concluded that the linear approximation is a good indicator of the distance a bleached wave penetrates an absorbing cell. This model was also benched marked against the quasi two level model. In the limit of high system pressure the simulated model converged to the same population inversion as that of the quasi two level regime. Finally, within the quasi two level regime a closed analytic equation was developed to describe under what conditions the system would lase.

Acknowledgments

I would like the thank Dr. Perram and Dr. Bailey for seeing me through this process. Especially for teaching me the importance of using experimental intuition when developing and applying theoretical tools and methods.

Charlton D. Lewis, II

Table of Contents

Page

List of Figures

Figure Page

List of Tables

A THEORETICAL MODEL ANALYSIS ON ABSORPTION OF A THREE LEVEL DIODE PUMPED ALKALI LASER

I. Introduction

The purpose of this model is to explore the key aspects of absorption in a diode pumped alkali lasing (DPAL) system. The key performance parameter space will be explored and reduced to controllable aspects that will aid in the engineering of such a system. To date the United States Air Force has invested heavily in chemical lasing systems. Although lasing powers have been achieved to become both tactically and strategically valuable (megawatt class), the logistic footprint and finite magazines of deploying chemical lasing systems have become a cause to research other lasing systems. Research has since been turned toward achieving power levels on the order of 100kW with solid state lasers. Progress in attaining such power levels have not been as fast as some researchers have hoped. As a possible solution to this problem the Air Force Institute of Technology along with its technology partners have been tasked to see if a combination laser, one that is part solid state and part gas, could fit the requirements of being both cost effective and tactically viable. Many aspects must come together in order for this to happen. To date most research has been done experimentally through trial and error.

A DPAL system is in essence a gas electric hybrid laser. The lasing medium is a gaseous cell of alkali typically Rubidium, Cesium, or Sodium. The unique character of

alkali atoms, a single valence electron, allows its first two excited states to be taken advantage of. A diode electric laser is used to pump or excite the alkali atoms to its second excited state and then inert gases are introduced in to the cell to collisionally de-excite the alkali atoms to its first excited state. The energy released then as the atoms finally return to their ground state is in the form of coherent lasing light. One big advantage of this system is thermal control. The flow rate of the gaseous medium through the lasing cell can be controlled thereby at the same time removing heat from the DPAL system. However there exists the technical challenge of matching the bandwidth of the diode laser stacks to that of the absorption bandwidth of the alkali medium. This can be slightly alleviated by broadening the alkali absorption spectrum by running the cell at a high pressure.

It is the aim of this paper to create a theoretical tool to tackle one aspect of a DPAL laser, which is the absorption of light in the gas lasing medium. The problem is to first describe the absorption cross section of Cesium and Rubidium to the hyperfine structure level under various system temperatures and pressures. Second, is to solve for the rate at which populations in the three different energy levels change under various system conditions. This will allow the deduction of how the diode pump field photons are absorbed or attenuated by the alkali atoms under both saturated and unsaturated conditions. From these ideas a picture of what a bleached wave is and how it affects system absorbance will be explored. Next, these ideas will be extended to a quasi-two level model in which the two excited states are infinitely coupled or the system is operating at very high pressure. The last challenge will be to introduce a lasing field into the quasi-two level regime and derive an analytic equation that will determine if under

what system conditions is lasing possible. This model will be simulated in a computing environment to help DPAL researchers determine what parameters a full up system will most likely be sensitive to as well as determine certain configurations that would limit absorption or lasing performance. This is not intended to be a full model of a tactically capable system, but rather a component of what could become a full up model.

II. Theory

Chapter Overview

The theory chapter will be devoted to the explanation and derivation of the necessary physical theories that this model will use to simulate the absorption of light by alkali atoms. The theories contained in this chapter are chiefly used by atomic spectroscopist and rely heavily on physics of light and matter interaction as well as quantum mechanics and kinetics. First, the properties and structure of alkali atoms will be discussed to the necessary precision required of this model. Next, how light interacts with matter will be discussed to understand how and why a gas of alkali atoms would absorb incoming photons. Then, a simple discussion of how the systems of alkali atoms change behavior when foreign species, other atoms or molecules, interfere with the absorption of light. Lastly, to mimic real conditions the effects of uncertainty, temperature, and pressure must be dealt with if this model is going to be useful.

Alkali Atomic Structure

Properties and Energy Levels

According to the International Union of Pure and Applied Chemistry (IUPAC) the series of alkali metal atoms, lithium, sodium, potassium, rubidium, cesium, and francium, comprise of the first family of elements on the periodic table. What makes these elements chemically similar and which defines their family is the position of their valence electron: it solely occupies an S-orbital. This observation is critical to how the alkali metals interact with their surrounding environment. Table 1 below lists some basic physical properties of the alkali metals:

Table 1. Alkali Physical Properties

	Lithium	Sodium	Potassium	Rubidium	Cesium	Francium
Atomic Number	3	11	19	37	55	87
Atomic Weight (amu)	6.941	22.990	39.098	85.468	132.905	223
Melting Point (°C)	180.54	97.72	63.38	39.31	28.44	Unknown
Boiling Point (°C)	1342	883	759	688	671	Unknown
Specific Heat Capacity (J/mol·K)	24.860	28.230	29.597	31.06	32.210	Unknown
Nuclear Spin	3/2	3/2	3/2	3/2(87) 7/2 (85)	7/2	3/2
Ionization Limit (kJ/mol)	520.2	495.8	418.8	403.0	375.7	Unknown

The similarity of these alkali atoms to the simplest atom, hydrogen, makes it easy to understand the energy levels of these atoms. The hydrogen atom consists of one electron orbiting one proton. Likewise the alkali metals consist of a positively charged core, the protons in the nucleus plus the inner electrons add to +1 charge, with a single electron inhabiting the outermost orbit. First, start with the nonrelativistic Hamiltonian operator describing the energy of the valence electron for the Hydrogen Atom:

$$\widehat{\mathbf{H}} = \frac{\hbar^2}{2m_e}\nabla^2 - \frac{e^2}{r}\widehat{\mathbf{r}} \tag{1.1}$$

where,

ħ = Planck's constant

m_e = mass of the electron (kg)

e = charge of the electron (coulomb)

r = distance separating proton and electron (m)

The electron experiences the familiar Coulomb potential which in this case is also spherically symmetrical. Second, cast the operator into spherical-polar coordinates. The time independent Schrodinger equation, $H\Psi=E\Psi$, can now be solved using the common separation of variables method. The solution for both the energy eigenstates and the normalized wavefunctions are as follows:

$$E_n = \frac{-m_e e^4}{2\hbar^2 n^2} \tag{1.2}$$

$$\Psi_{nlm}(\rho,\theta,\phi) = -\left\{\frac{\alpha^3(n-l-1)!}{2n\left[(n+1)!\right]^3}\right\}^{1/2} e^{-\rho/2}\rho^l L_{n+l}^{2l+1}(\rho)Y_l^m(\theta,\phi) \tag{1.3}$$

where,

n = electronic energy level quantum number

l, m = rotational energy level quantum numbers

$\alpha = \frac{2}{na_0}r$, a_0 = Bohr Radius

$\rho = \frac{2r}{na_0}$

$L_{n+l}^{2l+1}(\rho)$: Associated Laguerre Polynomials

$Y_l^m(\theta,\phi)$: Normalized Spherical Harmonics

The probability distributions of these wavefunctions give rise to the familiar electron orbitals learned in basic chemistry, s, p, d, f, etc.

The alkali metal elements can be cast into the same analytical ansatz as the hydrogen atom. The outermost electron of the alkalis experience the same spherical Coulomb potential as that of hydrogen. As stated before adding both the protons and electrons, excluding the valence electron, add up to a charge of +1. Noticing this trend the energy levels follow the same functional form, eqn. 1.2, as that of hydrogen with the following modifications:

$$E_{n,l} = \frac{-m_e e^4 \tilde{Z}^2}{2\hbar^2 (n - \delta_{n,l})^2} \tag{1.4}$$

where, $\tilde{Z}$ = Z – N +1, Z is the number of protons in the nucleus, and N is the number of electrons. The parameter $\delta_{n,l}$ contains corrections factors that account for the shift from hydrogen behavior. The first correction is $\alpha(l)$, the quantum defect factor, which is a function of the valence electron's orbital momentum value. As the electron orbits the core of protons and electrons it is quite possible that as higher angular momentum states are achieved the distance in which the electron penetrates the core will be greater. This leads to the second correction factor $\beta(l)$ which accounts for the fact that as the electron burrows into the core it experiences less shielding from the core electrons and so the Coulomb potential looks less classical. This is particularly important the closer the valence electron gets to the nucleus. The final form of this correction parameter is,

$$\delta_{n,l} = \alpha(l) + \frac{\beta(l)}{n^2} \tag{1.5}$$

Table 2. Quantum defect parameters for Li, Na, K, Rb, and Cs

	l =	0	1	2	3
Li		0.40	0.04	0.00	0.00
Na		1.35	0.85	0.01	0.00
K		2.19	1.71	0.25	0.00
Rb		3.13	2.66	1.34	0.01
Cs		4.06	3.59	2.46	0.02

Fine Structure Splitting

Another important phenomenon for the complete picture of the alkali atom structure is the coupling of both the spin and orbital angular momentum of the electron. For the hydrogen atom this spin-orbit (SO) coupling can be understood in a semi-classically way by noting that in the electron's rest frame the proton is orbiting the electron and this movement leads to current. This current in turn invokes a magnetic field and the electron's spin then couples to this field. However, since SO coupling is inherently a relativistic phenomenon it is natural to start with the Dirac equation that is appropriate for spin ½ particles i.e. electrons.

Start with the classical relativistic energy as prescribed by Einstein:

$$\mathcal{H} = (c^2 p^2 + m_0{}^2 c^4)^{1/2} \tag{1.6}$$

where,

c = speed of light (m/sec)

p = momentum (kg·m/sec)

m_0 = rest mass (kg)

When this Hamiltonian is substituted into the Schrodinger equation and the square root expanded in a series of the momentum, it treats time and space asymmetrically which cannot be the case since time and space are symmetric in special relativity. Therefore a modification must be performed first so that they become symmetric again.

This modification involves transforming the term in the parentheses of equation 1.6 to a perfect square. In this way the Schrodinger equation will be both linear in space and time:

$$\begin{aligned} c^2P^2 + {m_0}^2c^4 &= (ca_xP_x + ca_yP_y + ca_zP_z + \beta m_0c^2)^2 \\ &= (c\boldsymbol{\alpha}\cdot\mathbf{P} + \beta m_0c^2)^2 \end{aligned} \tag{1.7}$$

The constraints imposed by this method give the following requirements for α and β:

$$\begin{aligned} \alpha_i^2 = \beta^2 = 1 \qquad & (i = x, y, z) \\ \alpha_i\alpha_j + \alpha_j\alpha_i = \left[\alpha_i, \alpha_j\right]_+ = 0 \qquad & (i \neq j) \\ \alpha_i\beta + \beta\alpha_i = \left[\alpha_i, \beta\right]_+ = 0 & \end{aligned} \tag{1.8}$$

In order for H to remain Hermitian the α, β matrices must be themselves Hermitian as well as being traceless and having eigenvalues of ±1. These three requirements mean that the matrices that complete the perfect square of the relativistic Hamiltonian must be 4x4.

$$\boldsymbol{\alpha} = \begin{bmatrix} 0 & \boldsymbol{\sigma} \\ \boldsymbol{\sigma} & 0 \end{bmatrix},\ \boldsymbol{\beta} = \begin{bmatrix} \mathbf{I} & 0 \\ 0 & -\mathbf{I} \end{bmatrix} \tag{1.9}$$

The choice of what α, β are not unique since they can be transformed by a matrix that is unitary. The **σ** are the familiar 2x2 Pauli matrices and the identity matrices are 2x2. With such parameters defined Paul Dirac's equation can be fully realized:

$$i\hbar \frac{\partial |\psi\rangle}{\partial t} = (c\boldsymbol{\alpha} \cdot \hat{\mathbf{P}} + \boldsymbol{\beta} m_0 c^2) |\psi\rangle \tag{1.10}$$

The state vectors are now a four-component object rather than the two-component object familiar in non-relativistic quantum mechanics. However the energy eigenstates look vastly familiar with the modification that it contains two two-compnent spinors, χ and Φ:

$$\psi(t) = \begin{bmatrix} \chi \\ \Phi \end{bmatrix} e^{-iEt/\hbar} \tag{1.11}$$

Using the well-known time-independent Schrodinger equation the spin orbit interaction will naturally fall out as long as orders of the equation are expanded out to $(v/c)^4$. First, start by inserting the Coulomb potential, $V = -e^2 / r$, into the relativistic Hamiltonian which will yield a set of coupled spinor equations. The first spinor will describe the simple case of an electron orbiting a fixed proton. The second spinor contains information about a positron which is not of interest in this paper.

$$\begin{bmatrix} E - V - m_0 c^2 & -c\boldsymbol{\sigma} \cdot \mathbf{P} \\ -c\boldsymbol{\sigma} \cdot \mathbf{P} & E - V - m_0 c^2 \end{bmatrix} \begin{bmatrix} \chi \\ \Phi \end{bmatrix} = 0 \tag{1.12}$$

Solving for Φ and then inserting into the equation for χ will yield an uncoupled equation in χ only:

$$(E - V - m_0 c^2)\chi = c\boldsymbol{\sigma} \cdot \mathbf{P} \left[\frac{1}{E - V + m_0 c^2} \right] c\boldsymbol{\sigma} \cdot \mathbf{P} \chi \tag{1.13}$$

Now a couple of approximations involving the total energy, both kinetic and rest, can be made to recover the non-relativistic Schrodinger equation. Define the Schrodinger energy, E_s, as the total energy minus the rest energy. If we add one unit of rest mass energy to the total energy this relation appears:

$$E + m_0 c^2 = E_s + 2m_0 c^2 \tag{1.14}$$

At very low speeds compared to the speed of light the Schrodinger energy is much less than the rest energy and so:

$$E + m_0 c^2 \cong 2m_0 c^2 \tag{1.15}$$

This allows the denominator in equation 1.13 to be approximated as $2m_0c^2$ assuming the potential doesn't make any appreciable contributions. Solving for the electron spinor the standard Schrodinger equation is recovered.

$$\begin{aligned} E_s\chi &= \left[\frac{(\boldsymbol{\sigma}\cdot\mathbf{P})^2}{2m_0}+V\right]\chi \\ &= \left[\frac{P^2}{2m_0}+V\right]\chi \end{aligned} \tag{1.16}$$

However in order to see the fine structure the denominator in equation 1.13 has to be expanded to P^4 or $(v/c)^4$.

$$\begin{aligned} \frac{1}{E-V+m_0c^2} &= \frac{1}{E_s-V+2m_0c^2} = \frac{1}{2m_0c^2}\left(1+\frac{E_s-V}{2m_0c^2}\right)^{-1} \\ &\cong \frac{1}{2m_0c^2}\left(1-\frac{E_s-V}{2m_0c^2}\right) = \frac{1}{2m_0c^2}-\frac{E_s-V}{4m_0^2c^4} \end{aligned} \tag{1.17}$$

Inserting this back into equation 1.13 it begins to look closer to an analyzable Hamiltonian:

$$E_s\chi = \left[\frac{P^2}{2m_0}+V-\frac{\boldsymbol{\sigma}\cdot\mathbf{P}(E_s-V)\boldsymbol{\sigma}\cdot\mathbf{P}}{4m_0^2c^2}\right]\chi \tag{1.18}$$

If the quantity $E_s - V$ acted directly on χ the first order solution could simply be substituted. However since this is not the case a few manipulations using the commutator can rectify the situation.

$$\begin{aligned}(E_s - V)\boldsymbol{\sigma}\cdot\mathbf{P}\chi &= \boldsymbol{\sigma}\cdot\mathbf{P}(E_s - V)\chi + \boldsymbol{\sigma}\cdot[E_s - V, \mathbf{P}]\chi \\ &= (\boldsymbol{\sigma}\cdot\mathbf{P})\frac{P^2}{2m_0}\chi + [\mathbf{P}, V]\chi\end{aligned} \tag{1.19}$$

Equation 1.13 now becomes and equation in which the Hamiltonian has two familiar terms and three terms due solely to relativity:

$$\begin{aligned}E_s\chi &= \left\{\frac{P^2}{2m_0} + V - \frac{P^4}{8{m_0}^3c^2} - \frac{i\boldsymbol{\sigma}\cdot\mathbf{P}\times[\mathbf{P}, V]}{4{m_0}^2c^2} - \frac{\mathbf{P}\cdot[\mathbf{P}, V]}{4{m_0}^2c^2}\right\}\chi \\ &= \hat{\mathbf{H}}\chi\end{aligned} \tag{1.20}$$

The third term is the relativistic correction to the kinetic energy, the fourth term contains the correction that is sought after, the SO coupling energy, and the fifth term is known as the Darwin correction. The evaluation of the SO coupling term is straight forward:

$$\begin{aligned}\hat{\mathbf{H}}_{S.O.} &= -\frac{i\boldsymbol{\sigma}\cdot\hat{\mathbf{P}}\times\left[\hat{\mathbf{P}},V(\hat{\mathbf{r}})\right]}{4m_0{}^2c^2} \\ &= -\frac{i\boldsymbol{\sigma}\cdot\hat{\mathbf{P}}\times\left[-i\hbar\nabla(-e^2/\hat{\mathbf{r}})\right]}{4m_0{}^2c^2} \\ &= \frac{\hbar e^2}{4m_0{}^2c^2r^3}\boldsymbol{\sigma}\cdot\hat{\mathbf{r}}\times\hat{\mathbf{P}} \\ &= \frac{e^2}{2m_0{}^2c^2r^3}\hat{\mathbf{S}}\cdot\hat{\mathbf{L}}\end{aligned} \tag{1.21}$$

For the Alkali metals this interaction causes a splitting of the energy levels. To compute the energy corrections one has to move to a basis that will completely diagonalize H. In this case the total angular momentum basis, J=L+S, is sufficient to understand what happens at the fine structure level. The energy corrections are proportional to the quantity:

$$E_{S.O.} \approx \zeta(r)\cdot\left[J\left(J+1\right)-L(L+1)-S(S+1)\right] \tag{1.22}$$

The valence electrons in each Alkali atom in the ground state are contained in an s-orbital. So their angular momentum numbers are J = 1/2, L = 0, and S = ±1/2. As such no fine splitting occurs in the ground state. Once the electron is promoted to the next energy level it finds itself in a p-orbital with momentum numbers J = 3/2, 1/2, L = 1, and S = ±1/2. So an Alkali valence electron when excited to the next energy level has two fine structure levels to ascend towards. This gives rise to the characteristic doublet absorption lines seen in the alkali metals.

Hyperfine Structure Splitting

The hyperfine structure will be the furthest this paper needs to go into the internal structure of the atom. Qualitatively the hyperfine structure is brought about by the same scheme the SO correction came out of: interaction of electromagnetic fields and particle spin. The fine structure coupled the spin of the electron with its orbital momentum via an electromagnetic interaction. However just as the electron has intrinsic spin so do the particles that makes up the nucleus. This is called nuclear spin and is typically labeled I. The nucleus can be attributed a magnetic moment and therefore depending on its size will have multi-pole moments describing its field. So the picture looks as such for the hyperfine interaction:

1.) The magnetic moment of the nucleus will interact with the magnetic field produced by the current of the orbiting electron.
2.) Both the nucleus and electron by virtue of their spin produce magnetic moments. As such multi-pole interactions occur.
3.) Lastly, there is what is known as Fermi's contact term which describes the interaction of the electrons magnetic moment with the magnetic field inside the nucleus to include singularities that exist inside the particles.

Once again we will take the simple case of the hydrogen atom, determine the hyperfine Hamiltonian from first principles, and then determine what it will take to extend to alkali systems.

The Hamiltonian of an electron in the presence of a magnetic field produced by a proton is:

$$\hat{\mathbf{H}} = \frac{1}{2m_e}\left[\hat{\mathbf{P}} - e\mathbf{A}_\mathbf{I}(\hat{\mathbf{r}})\right]^2 - eV_\mathbf{I}(\hat{\mathbf{r}}) - 2\mu_B\left(\frac{\hat{\mathbf{S}}}{\hbar}\right)\cdot\nabla\times\mathbf{A}_\mathbf{I}(\hat{\mathbf{r}}) \tag{1.23}$$

where,

A_I = Vector potential of nucleus

μ_B = The Bohr Magneton

V_I = electric potential of the nucleus

Note that the final term is the coupling of the electron's spin with the magnetic field of the nucleus. The vector potential is related to the magnetic dipole moment by:

$$A_I(\hat{\mathbf{r}}) = \frac{\mu_0}{4\pi}\frac{\mathbf{M}_\mathbf{I}\times\hat{\mathbf{r}}}{r^3} \tag{1.24}$$

where,

M_I = magnetic dipole moment of the nucleus

μ_0 = magnetic permeability

Inserting equation 1.24 into equation 1.23 and ignoring any quadratic terms of the vector potential the first term in 1.23 becomes:

$$\hat{\mathbf{P}}\cdot\mathbf{A}_\mathbf{I}(\hat{\mathbf{r}}) + \mathbf{A}_\mathbf{I}(\hat{\mathbf{r}})\cdot\hat{\mathbf{P}} = \frac{\mu_0}{4\pi}\left\{\frac{\hat{\mathbf{P}}\cdot(\mathbf{M}_\mathbf{I}\times\hat{\mathbf{r}})}{r^3} + \frac{(\mathbf{M}_\mathbf{I}\times\hat{\mathbf{r}})\cdot\hat{\mathbf{P}}}{r^3}\right\} \tag{1.25}$$

The magnetic moment commutes with both **P** and **R** since it only involves the spin operator so the first and second terms of 1.25 can be rewritten as:

$$\frac{\hat{\mathbf{P}}\cdot\left(\mathbf{M_I}\times\hat{\mathbf{r}}\right)}{r^3}=\frac{\hat{\mathbf{L}}\cdot\mathbf{M_I}}{r^3}$$
$$\frac{\left(\mathbf{M_I}\times\hat{\mathbf{r}}\right)\cdot\hat{\mathbf{P}}}{r^3}=\frac{\mathbf{M_I}\cdot\hat{\mathbf{L}}}{r^3} \tag{1.26}$$

One just has to be careful when using cross product identities not to upset the order of multiplication between **P** and **R** since they do not commute like the scalar operator |**r**|. As such the first two terms in equation 1.23 become something that is analyzable by inspection:

$$\hat{\mathbf{H}}_{hf}^{L}=-\frac{\mu_0}{4\pi}\frac{e}{2m_e}2\frac{\mathbf{M_I}\cdot\hat{\mathbf{L}}}{r^3}=-2\mathbf{M_I}\cdot\mathbf{B_L} \tag{1.27}$$

Now it is clear that the magnetic moment of the nucleus is coupling to the magnetic field due to the current of the electron.

The last two interactions, the dipole-dipole and Fermi interaction, are contained in the last term of equation 1.23. This involves knowing the magnetic field both outside and inside the proton. For the field outside the field is simply that of a dipole field. If we align the magnetic dipole moment in the z-direction the dipole field is:

$$B_x=\frac{\mu_0}{4\pi}3M_I\frac{xy}{r^5}$$
$$B_x=\frac{\mu_0}{4\pi}3M_I\frac{yz}{r^5} \tag{1.28}$$
$$B_x=\frac{\mu_0}{4\pi}M_I\frac{3z^2-r^2}{r^5}$$

Now to complete the dipole interaction term we take the components of the electronic spin operator and dot product them into equation 1.28. Also by definition $\mathbf{M_I}$ is in the z-direction so:

$$\widehat{\mathbf{H}}_{hf}^{dip} = 2\mu_B \frac{\mu_0}{4\pi}\left(\frac{\widehat{\mathbf{S}}}{\hbar}\right)\cdot\nabla\times A_I(\widehat{\mathbf{r}}) = \frac{\mu_0 2\mu_B}{4\pi\hbar r^3}\left\{\widehat{\mathbf{S}}\cdot\mathbf{M_I} - 3\frac{\left(\widehat{\mathbf{S}}\cdot\widehat{\mathbf{r}}\right)\left(\mathbf{M_I}\cdot\widehat{\mathbf{S}}\right)}{r^2}\right\} \tag{1.29}$$

The electronic spin is now coupled to the nuclear spin, in this case the proton.

The magnetic field inside the proton is calculated by adding the flux outside the radius of the proton, ρ_0, the flux inside the radius, setting them equal to zero and solving for B_i:

$$B_i = \frac{\mu_0}{4\pi} M_I \frac{2}{\rho_0^3} \tag{1.30}$$

To understand the effects of this term insert 1.30 into the last term of equation 1.23 and use the $|n,l,m,s\rangle$ representation to expand:

$$\begin{aligned}&\langle n,l,m,s|\frac{-\mu_0 4\mu_B M_I}{4\pi\hbar{\rho_0}^3}|n',l',m',s'\rangle = \\ &\frac{-\mu_0 4\mu_B M_I}{4\pi\hbar{\rho_0}^3}\langle s|S_z|s'\rangle\iiint_{r\le\rho_0} d^3r\varphi^*_{n,l,m}(\mathbf{r})\varphi_{n',l',m'}(\mathbf{r})\end{aligned} \tag{1.31}$$

As ρ_0 goes to zero so does the volume element, $\frac{4}{3}\pi\rho_0^3$, and so the integral becomes a delta function at **r** = 0. Thus the last hyperfine correction:

$$\hat{\mathbf{H}}_{hf}^{Fermi} = \frac{-\mu_0}{4\pi}\frac{8\pi}{3}\mathbf{M}_{\mathbf{I}} \cdot \left(\frac{2\mu_B \hat{\mathbf{S}}}{\hbar}\right)\delta(\hat{\mathbf{r}}) \tag{1.32}$$

This completes what is known as the hyperfine structure of the Hydrogen atom:

$$\hat{\mathbf{H}}_{hf} = \hat{\mathbf{H}}_{hf}^{L} + \hat{\mathbf{H}}_{hf}^{dip} + \hat{\mathbf{H}}_{hf}^{Fermi} \tag{1.33}$$

What makes this analysis so straight forward is that the nucleus contains only one proton and so only the dipole term needs to be considered. The number of multipoles that must be included in the above analysis must be less than or equal to twice the nuclear spin. Equation 1.23 would then contain extra terms in both the electric potential and magnetic potential. For the alkali metals this is definitely the case and though the derivation will not be repeated the same process will yield the hyperfine Hamiltonian for alkali metals (using a suitable angular momentum basis):

$$\hat{\mathbf{H}}_{hfs} = A_{hfs}\hat{\mathbf{I}}\cdot\hat{\mathbf{J}} + B_{hfs}\frac{3(\hat{\mathbf{I}}\cdot\hat{\mathbf{J}})^2 + \frac{3}{2}(\hat{\mathbf{I}}\cdot\hat{\mathbf{J}}) - I(I+1)J(J+1)}{2I(2I-1)J(2J-1)} + C_{hfs}\frac{10(\hat{\mathbf{I}}\cdot\hat{\mathbf{J}})^3 + 20(\hat{\mathbf{I}}\cdot\hat{\mathbf{J}})^2 + 2(\hat{\mathbf{I}}\cdot\hat{\mathbf{J}})\left[I(I+1)+J(J+1)+3\right] - 3I(I+1)J(J+1) - 5I(I+1)J(J+1)}{I(I-1)(2I-1)J(J-1)(2J-1)} \tag{1.34}$$

where A_{hfs} is the magnetic dipole constant, B_{hfs} is the electric quadrupole constant, and C_{hfs} is the magnetic octupole moment. Below in Table x are the multipole moments of Cesium and Rubidium.

Table 3. Hyperfine Multipole constants for Cesium and Rubidium

Moment	Cesium	Rubidium 85	Rubidium 87
A $S_{1/2}$	h·2.2981 GHz	h·1.0119 GHz	h·3.4173 GHz
A $P_{1/2}$	h·291.9201 MHz	h·120.527(6) MHz	h·408.328(2) MHz
A $P_{3/2}$	h·50.2882 MHz	h·25.0020 MHz	h·84.7185 MHz
B $P_{3/2}$	-h·0.4934 MHz	h·25.790(9) MHz	h·12.4965 MHz
C $P_{3/2}$	h·0.0560 MHz	-	-

This completes the section on the internal structure of atom important to this paper. Understanding the simple Hydrogen system allowed us to adapt equations to fit the alkali elements. From a coarse perspective we saw that the alkali metal energy levels can be adapted to that of what the hydrogen's exact levels are. Since the alkali metals and hydrogen have only one valence electron orbiting in a ground state s-orbital this allowed correction factors to be inserted to describe the alkalis. At a fine level the intrinsic spin of the electron coupled to the magnetic field created by the orbiting nucleus (in the electron's rest frame). Using the ideas from special relativity and combining them with the ideas from quantum mechanics both spin and SO coupling were revealed to be a natural phenomena of a more accurate description of reality rather than just using ad hoc semi-classical explanations. Lastly, the hyperfine structure was the result of including the magnetic potential into the Hamiltonian of the electron. In the case of hydrogen it was enough to use only the dipole moment since it is the only moment a proton has. However when moving to the alkali atoms the nuclei no longer present a simple electric and magnetic field. To rectify the situation one has to begin by expanding both the vector and

electric potentials in to their multi-pole form. Then following the same analysis as in the hyperfine hydrogen analysis, a hyperfine structure is revealed to involve the magnetic dipole and octupole as well as the electric quadrupole. Figures 1-6 capture the internal structure of Cs, Rb85, and Rb87 and their energy levels.

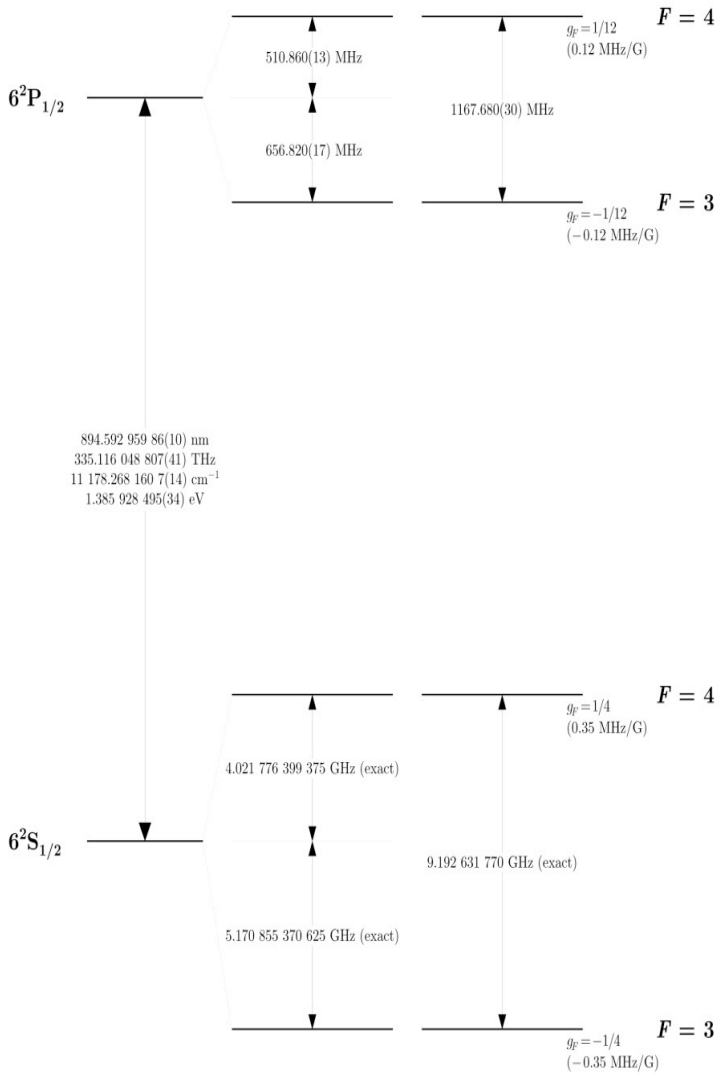

Figure 1. Cs D1 Energy Level Diagram

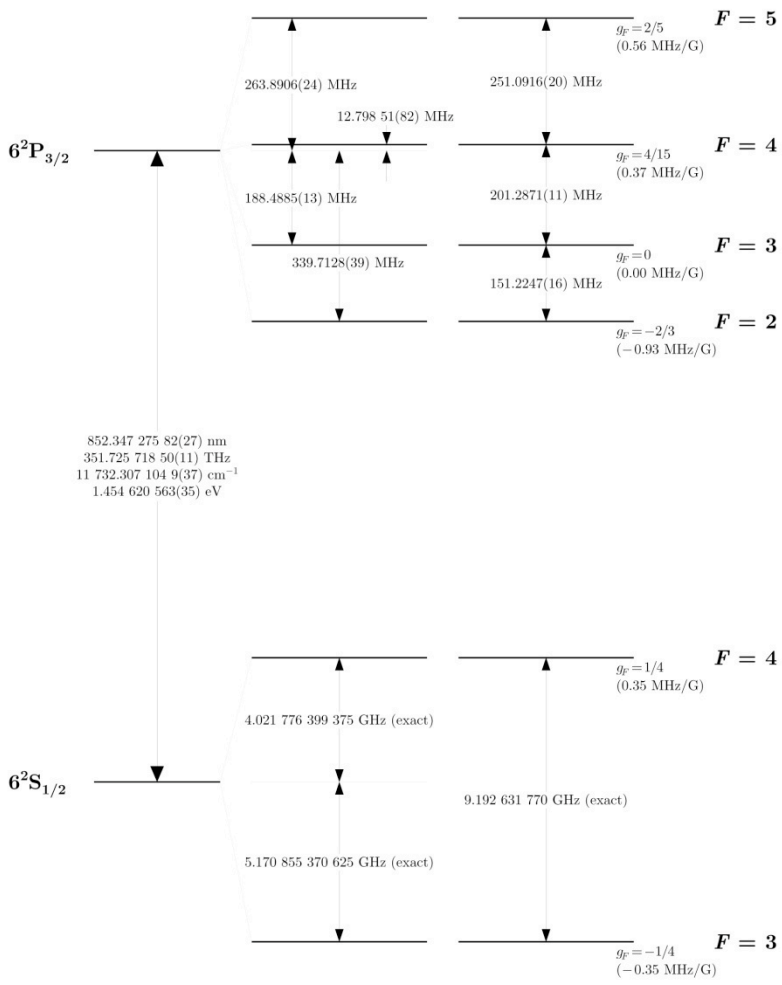

Figure 2. Cs D2 Energy Level Diagram

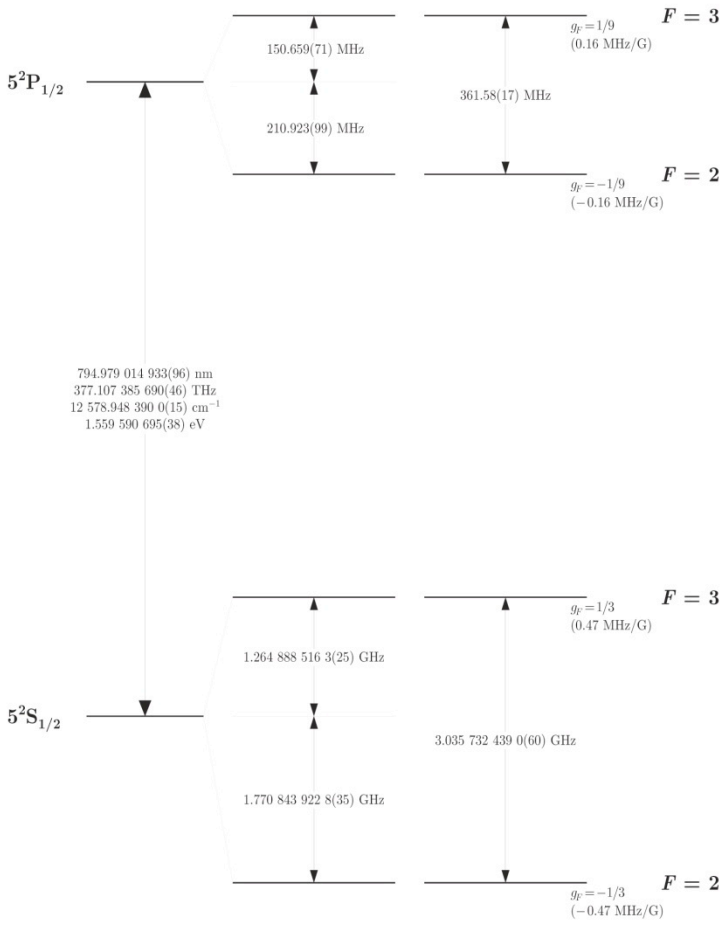

Figure 3. Rb85 D1 Energy Level Diagram

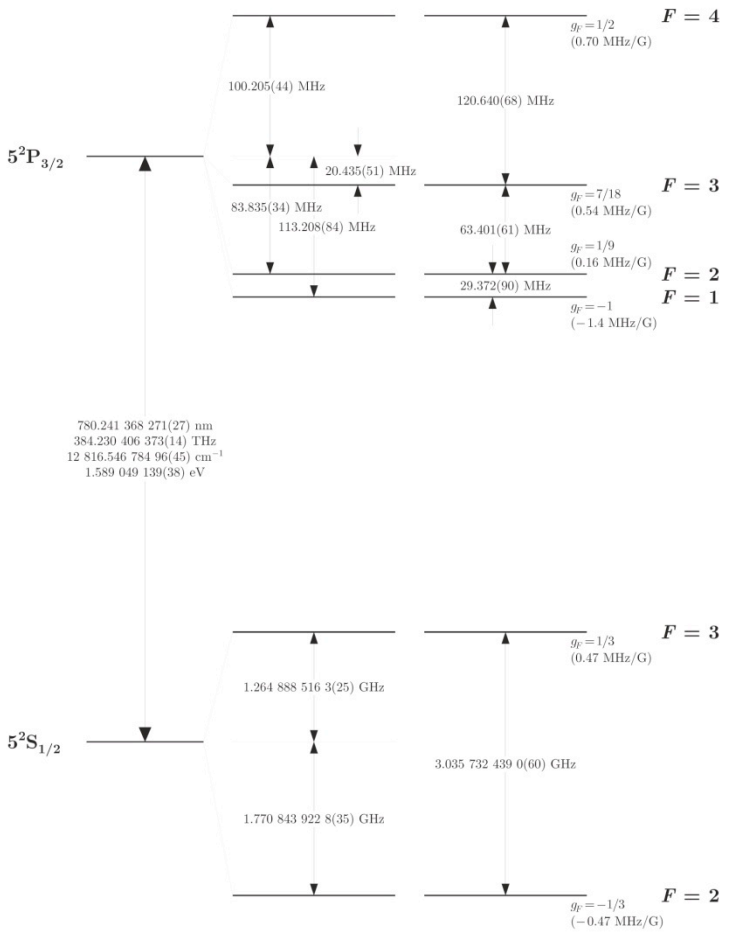

Figure 4. Rb85 D2 Energy Level Diagram

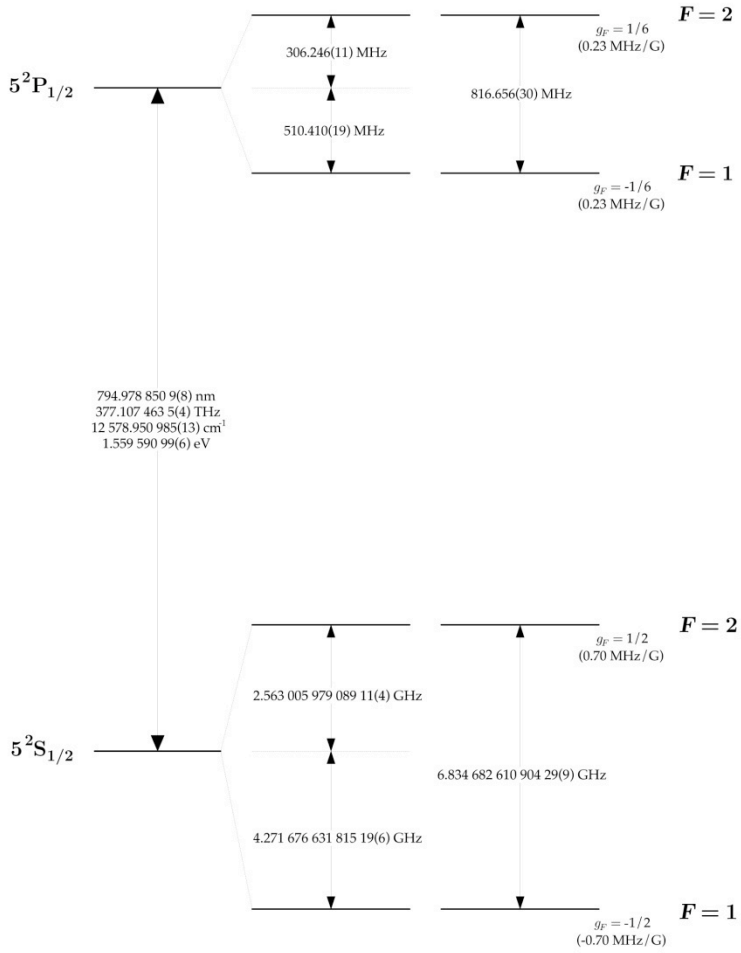

Figure 5. Rb87 D1 Energy Level Diagram

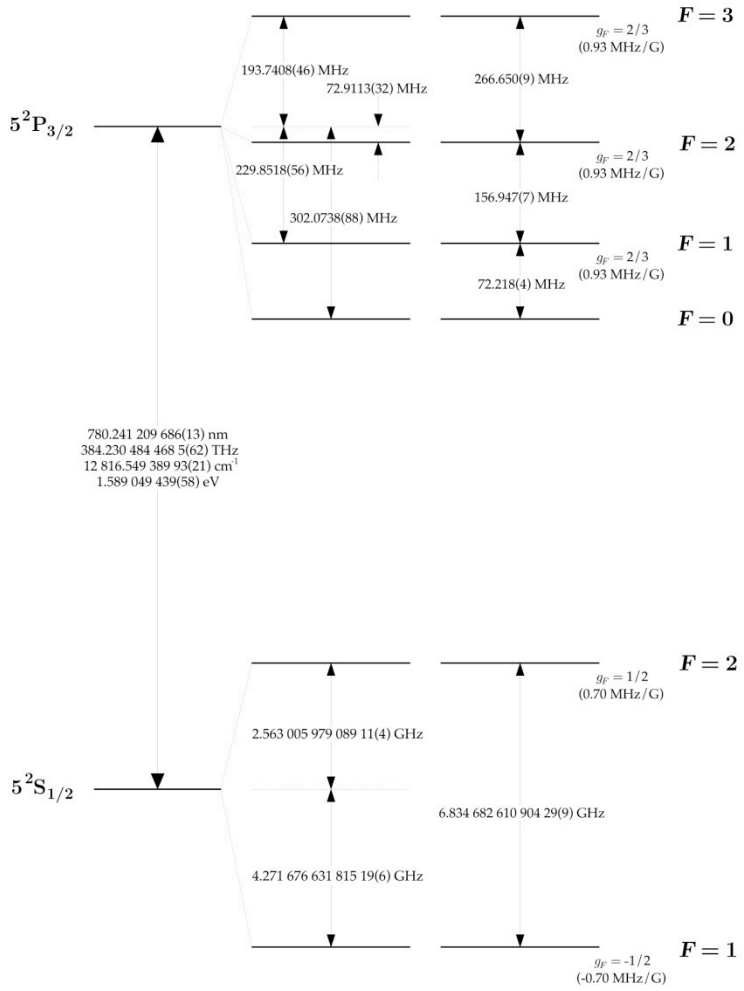

Figure 6. Rb87 D2 Energy Level Diagram

Interaction of Light and Matter

Time Dependent Perturbation Theory (TDPT)

Once the energy levels in the alkali atom structures have been defined to the hyperfine level a number of questions arise. The most relevant question is how does one physically promote an electron to a higher energy state? The obvious answer is to add energy to the system. We could collisionally excite the atoms by bombarding them with an inert gas or perhaps heat the system up so that elevated states become the new equilibrium. For the case of a DPAL system the alkali atoms are promoted through what is known as stimulated absorption. We will consider an electromagnetic wave impingent on the alkali atom. A dipole moment can be specified between the valence electron and the nucleus and it is this dipole moment that will interact with electromagnetic wave. In the case of a DPAL system this light is provided by the diode laser pump source. There is more to the story than just promotion. Two other questions naturally arise as well 1.) are all hyperfine transitions allowed and 2.) how strong do the transitions couple to the electromagnetic radiation? All these questions can be answered by moving to a time-dependent regime. This is necessary because the system is no longer in a stationary state. Before the diode is turned on the system is unperturbed. As soon as the diode is turned on at some time, t, a perturbing Hamiltonian must be introduced into the system for a length of time equal to how long the perturbations lasts. Once the perturbation is gone the system will relax back into its unperturbed state. TDPT will be used to explore the answers to these questions.

The starting point for TDPT is the time dependent Schrodinger equation. Assume that the time dependency is parameterized by a strength factor λ:

$$i\hbar \frac{d}{dt}\left|\psi(t)\right\rangle = \widehat{\mathbf{H}}(t)\left|\psi(t)\right\rangle \tag{1.35}$$

$$\widehat{\mathbf{H}}(t) = \widehat{\mathbf{H}}_0 + \lambda \widehat{\mathbf{H}}_1(t) \tag{1.36}$$

The most important question that can be asked in this regime is what is the probability of the initial state, Ψ_i , transitioning to a final state, Ψ_f? In the case of the excitation of an alkali atom what is the probability that a photon will excite an electron from the ground state to an excited state?

Start by expressing the state ket as an expansion in its own complete basis:

$$\left|\psi(t)\right\rangle = \sum_n c_n(t)\left|n^0\right\rangle \tag{1.37}$$

If H_1 is not present we can show with the help of the propagator the solution to $c_n(t)$ as:

$$\begin{aligned}
&\left|\psi(t)\right\rangle = U(t)\left|\psi(0)\right\rangle \\
&\sum_n c_n(t)\left|n^0\right\rangle = U(t)\left|\psi(0)\right\rangle \\
&\sum_n c_n(t)\left|n^0\right\rangle = \sum_n e^{-iE_n^0 t/\hbar}\left|n^0\right\rangle\left\langle n^0\right|c_n(0)\left|n^0\right\rangle \\
&c_n(t) = c_n(0)e^{-iE_n^0 t/\hbar}
\end{aligned} \tag{1.38}$$

However when H_1 is present there must be another term in the state function that evolves in time. Taking this into account the state function can be written as:

$$\left|\psi(t)\right\rangle = \sum_n b_n(t)e^{-iE_n^0 t/\hbar}\left|n^0\right\rangle \tag{1.39}$$

If the $b_n(t)$ change it is because of H_1 and not H_0. Equation 1.39 can now be substituted into equation 1.35 to get the following:

$$\left[\sum_n ih\dot{b}_n(t) - \lambda\hat{\mathbf{H}}_1(t)b_n(t)\right]e^{-iE_n^0 t/\hbar}\left|n^0\right\rangle = 0 \tag{1.40}$$

Next take the dot product of equation 1.40 with the final state $\left|f(t)\right\rangle = e^{-iE_n^0 t/\hbar}\left|f^0\right\rangle$ and solve for b_f:

$$\left\langle f^0\right|e^{iE_f^0 t/\hbar}\left[\sum_n i\hbar\dot{b}_n(t) - \lambda\hat{\mathbf{H}}_1(t)b_n(t)\right]e^{-iE_n^0 t/\hbar}\left|n^0\right\rangle = 0 \tag{1.41}$$

$$i\hbar\dot{b}_f = \sum_n \left\langle f^0\right|\lambda\hat{\mathbf{H}}_1(t)\left|n^0\right\rangle b_n(t)e^{i\omega_{fn}t} \tag{1.42}$$

where $\omega_{fn} = \dfrac{E_f^0 - E_n^0}{\hbar}$.

No approximations up till now have been used. As with many methods in quantum mechanics we want to see if higher order corrections affect zeroth order solutions and so the expansion coefficients themselves will be expanded in a power series. This is the first introduced approximation for TDPT:

$$\begin{aligned} b_n(t) &= b_n^{(0)}(t) + b_n^{(1)}(t)\lambda + b_n^{(2)}(t)\lambda^2 + \ldots \\ &= \sum_{r=0}^{\infty}\lambda^r b_n^{(r)}(t) \end{aligned} \tag{1.43}$$

Once equation 1.43 is substituted into equation 1.42 we find that:

$$\sum_{r=0}^{\infty} \lambda^r \dot{b}_f^{(r)}(t) = \sum_n \left\langle f^0 \left| \hat{\mathbf{H}}_1(t) \right| n^0 \right\rangle e^{i\omega_{fi}t/\hbar} \sum_{r=0}^{\infty} \lambda^{r+1} b_n^{(r)}(t) \tag{1.44}$$

Now like powers of r can be equated together and two conditions can be examined with the second leading to a recursion relation.

when r = 0,

$$i\hbar \dot{b}_f^{(0)}(t) = 0 \tag{1.45}$$

when r ≠ 0,

$$i\hbar \dot{b}_f^{(r)}(t) = \sum_n \left\langle f^0 \left| \hat{\mathbf{H}}_1(t) \right| n^0 \right\rangle e^{i\omega_{fi}t/\hbar} \sum_{r=0}^{\infty} b_f^{(r-1)}(t) \tag{1.46}$$

To compute the first order result the zeroth order result must be computed first. Equation 1.45 says that the zeroth order solution is a constant in time so pick to solution at t=0. In other words the initial state before the perturbation occurs:

$$b_f^{(0)}(0) = \delta_{ni} \tag{1.47}$$

Moving on to the first order result:

$$
\begin{aligned}
i\hbar\dot{b}_f^{(1)}(t) &= \sum_n \left\langle f^0 \left| \hat{\mathbf{H}}_1(t) \right| n^0 \right\rangle e^{i\omega_f t/\hbar} b_f^{(0)}(0) \\
&= \sum_n \left\langle f^0 \left| \hat{\mathbf{H}}_1(t) \right| n^0 \right\rangle e^{i\omega_f t/\hbar} \delta_{ni} \\
&= \left\langle f^0 \left| \hat{\mathbf{H}}_1(t) \right| i^0 \right\rangle e^{i\omega_f t/\hbar}
\end{aligned}
\tag{1.48}
$$

Integrating equation 1.48 the solution for the time evolved state up to first order is:

$$
\begin{aligned}
b_f(t) &= b_f^0(t) + b_f^1(t) \\
&= \delta_{fi} - \frac{i}{\hbar} \int_0^t \left\langle f^0 \left| \hat{\mathbf{H}}_1(t') \right| i^0 \right\rangle e^{i\omega_f t'/\hbar} dt'
\end{aligned}
\tag{1.49}
$$

The probability for transition from initial to final state is simply the absolute value of equation 1.49 squared. Now that a general formula for transition probability has been derived the form of H_1 will make it applicable to systems we are interested in, mainly the hydrogen atom and the excitation of alkali atoms in the presence of an electromagnetic field.

The Hamiltonian: Zeroth and First Order

We will look at the case of monochromatic light interacting with the simple hydrogen system. Although the hydrogen atom is neutral it contains a dipole moment by virtue of proton electron separation. As with any dipole phenomenon it will have a natural resonating frequency and it is this frequency that can couple to monochromatic light if and only if the natural frequency and frequency of radiation match. To begin we start with the relativistically invariant form of hydrogen in an electromagnetic field:

$$\hat{H} = \frac{1}{2m}\left(\hat{\mathbf{P}} - \frac{e}{c}\mathbf{A}(\hat{\mathbf{r}}) \right)^2 + \left(V(\hat{\mathbf{r}}) + e\phi \right) \tag{1.50}$$

where $\hat{\mathbf{A}}$ is the vector potential and ϕ the electric potential of the radiation field.

Expanding equation 1.50 and substituting into the Schrodinger Equation we find:

$$i\hbar \frac{d}{dt}|\psi\rangle = \left\{ \frac{1}{2m_e}\left(-\hbar^2\nabla^2 + i\hbar\nabla\cdot\mathbf{A} + 2i\hbar\frac{e}{c}\mathbf{A}\cdot\nabla + \frac{e^2}{c^2}|\mathbf{A}|^2 \right) + V(\hat{\mathbf{r}}) + e\phi \right\} |\psi\rangle \tag{1.51}$$

Utilizing the Coulomb Gauge equation 1.51 can be put in the form of:

$$\begin{aligned} \hat{\mathbf{H}}|\psi\rangle &= \left[H_0 + H_1(t) \right] |\psi\rangle \\ &= \left\{ \left[-\frac{\hbar^2}{2m_e} + V(\hat{\mathbf{r}}) \right] + \left[\frac{ie\hbar}{m_e c}\mathbf{A}\cdot\nabla + \frac{e^2}{2m_e c^2}|\mathbf{A}|^2 \right] \right\} |\psi\rangle \end{aligned} \tag{1.52}$$

So long as the magnetic field is not absurdly high the fourth term in equation 1.52 can be neglected. The form of the vector potential is both oscillatory in space and in time and can be written as a plane wave:

$$\mathbf{A}(\hat{\mathbf{r}}, t) = \mathbf{A}_0 e^{(-\omega t - \mathbf{k}\cdot\hat{\mathbf{r}})} \tag{1.53}$$

and the electric field is,

$$E(\mathbf{r}, t) = \frac{-1}{c}\frac{\partial \mathbf{A}}{\partial t} = -\omega \mathbf{A_0} e^{(-\omega t - \mathbf{k}\cdot\hat{\mathbf{r}})} \tag{1.54}$$

Periodic Perturbations

First, we shall treat the time dependence of the perturbation in equation 1.52 separately expressing $\mathbf{H_1}$ as:

$$\widehat{\mathbf{H}}_1(t) = \widehat{\mathbf{H}}_1 e^{-\omega t} \tag{1.55}$$

This will make the math more simplistic since sines and cosines which typically describe wave behavior in time can be expressed as exponentials. Suppose at t = 0 the hydrogen atom comes into contact with the perturbation described by 1.54 for a finite amount of time, t. This can now be handled by equation 1.49:

$$\begin{aligned} b_f^{(1)}(t) &= -\frac{i}{\hbar}\left\langle f^0 \left| \widehat{\mathbf{H}}_1 \right| i^0 \right\rangle \int_0^t e^{i\left(\omega_{fi}-\omega\right)t'} dt' \\ &= -\frac{i}{\hbar}\left\langle f^0 \left| \widehat{\mathbf{H}}_1 \right| i^0 \right\rangle \frac{e^{i\left(\omega_{fi}-\omega\right)t} - 1}{i\left(\omega_{fi}-\omega\right)} \end{aligned} \tag{1.56}$$

The probability of transition is the absolute value of equation 1.56 squared:

$$P_{i\to f} = \frac{1}{\hbar^2}\left|\left\langle f^0 \left| \widehat{\mathbf{H}}_1 \right| i^0 \right\rangle\right|^2 \left\{\frac{\sin\left[\left(\omega_{fi}-\omega\right)t/2\right]}{\left(\omega_{fi}-\omega\right)t/2}\right\}^2 t^2 \tag{1.57}$$

Equation 1.57 has a functional form of $sin^2(x)/x^2$ and if this is plotted we see that the probability will favor a transition based on the width of this function.

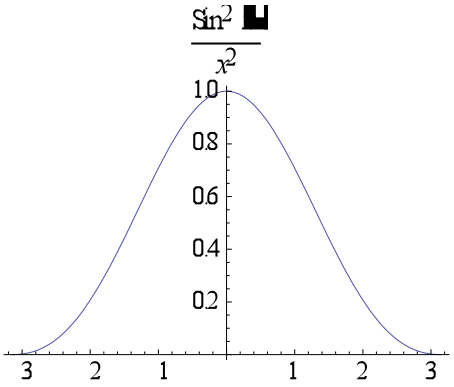

The function has a full width half maximum of about π. Let's consider this FWHM value to be the favorable transition threshold so that we can relate the denominator of 1.57 as:

$$\left|(\omega_{fi}-\omega)t/2\right| \le \pi \tag{1.58}$$

Multiply equation 1.58 by ħ so that energy units are used and solve for ω_{fi} to yield:

$$E_f^0 - E_i^0 = \hbar\omega\left(1 \pm \frac{2\pi}{\omega t}\right) \tag{1.59}$$

As long as $\omega t >> 2\pi$ and we know how to calculate initial and final energy levels we only need to use a frequency proportional to the energy difference to excite an electron.

Dipole Transition

Now that the temporal portion of the perturbation has been analyzed next the spatial portions which are contained in the matrix elements of equation 1.56 will yield information about what hyperfine transitions are allowed and their strength. The matrix elements are best resolved one component at a time.

$$\left\langle f^0 \left| \widehat{\mathbf{H}}_1 \right| i^0 \right\rangle = \left\langle f^0 \left| \frac{ie\hbar}{m_e c} \mathbf{A}_\mathbf{0} \cdot \nabla \right| i^0 \right\rangle = \sum_{q=1}^{3} \mathbf{A}_{\mathbf{0}q} \left\langle f^0 \left| \frac{ie\hbar}{m_e c} e^{ikz} \frac{\partial}{\partial q} \right| i^0 \right\rangle \qquad (1.60)$$

Next we introduce the *dipole approximation* which is first to expand the exponential in equation 1.60:

$$e^{ikz} = 1 + ik(z - z_0) - \frac{k^2}{2}(z - z_0)^2 + \ldots \qquad (1.61)$$

If the product of kz is much much less than 1 we only need to take the first term for the exponential. The constant k is equal to $\frac{2\pi}{\lambda}$ so for any wavelength that is greater than ultraviolet this approximation will remain valid. A more physical picture is this: over the length of the molecule or atom, which is on the order of angstroms, the spatial deviation of the electromagnetic wave hardly changes and can be approximated as a constant field. With this approximation in mind equation 1.60 becomes (see Appendix A):

$$\begin{aligned} \sum_{q=1}^{3} \mathbf{A}_{\mathbf{0}q} \left\langle f^0 \left| \frac{ie\hbar}{m_e c} e^{ikz} \frac{\partial}{\partial q} \right| i^0 \right\rangle &= \sum_{q=1}^{3} \mathbf{A}_{\mathbf{0}q} \left\langle f^0 \left| \frac{ie\hbar}{m_e c} \frac{\partial}{\partial q} \right| i^0 \right\rangle \\ &= \sum_{q=1}^{3} \frac{-e}{c} \omega_{fi} \mathbf{A}_{\mathbf{0}\,q} \left\langle f^0 \left| q \right| i^0 \right\rangle \end{aligned} \qquad (1.62)$$

Plugging this into equation 1.56 the final form for the probability transition is nearly complete:

$$P_{i\to f}=\frac{1}{\hbar^2}\left(\frac{e}{c}\right)^2\omega_0^2\left|A_0\right|^2\left|\left\langle f^0\left|\mathbf{r}\right|i^0\right\rangle\right|^2\left\{\frac{\sin\left[\left(\omega_{fi}-\omega\right)t/2\right]}{\left(\omega_{fi}-\omega\right)t/2}\right\}^2 t^2 \qquad (1.63)$$

The most important term in this transition probability lies in the matrix element of the transition. From these elements we can understand not only what transitions are allowed between arbitrary initial and final states, but also if the transition is allowed how strong will it be. The generalized theorem to calculate these matrix elements is the Wigner-Eckart Theorem which states:

$$\left\langle \alpha_2, j_2, m_2\left|T_k^q\right|\alpha_1, j_1, m_1\right\rangle=\frac{\left\langle \alpha_2, j_2\left|T_k\right|\alpha_1, j_1\right\rangle}{\sqrt{2j+1}}\left\langle j_2, m_2\left|k, q; j_1, m_1\right\rangle\right. \qquad (1.64)$$

where the T_k^q are spherical tensor operators, the α's represent all non-angular quantum numbers, and j,m are standard quantum numbers. We see that the angular dependence of the matrix elements are separated into the familiar Clebsch-Gordon Coefficients. This will be related to the strength of the transition and can easily be calculated from CG Tables. The remaining matrix element will give us the selection rule. Essentially it must be that in the reduced matrix element on right hand side of equation 1.64 $j_2 = j_1 \pm k$ or else no transition will take place. If we recognize the following:

$$\begin{aligned} \mathrm{X} &= \frac{T_1^{-1}-T_1^1}{\sqrt{2}} \\ \mathrm{Y} &= \frac{T_1^{-1}+T_1^1}{\sqrt{2}} \\ \mathrm{Z} &= \mathrm{T}_1^0 \end{aligned} \qquad (1.65)$$

and substitute r = x+y+z the Wigner-Eckart theorem can be used to compute transition strengths and allowed transitions.

Three Level System

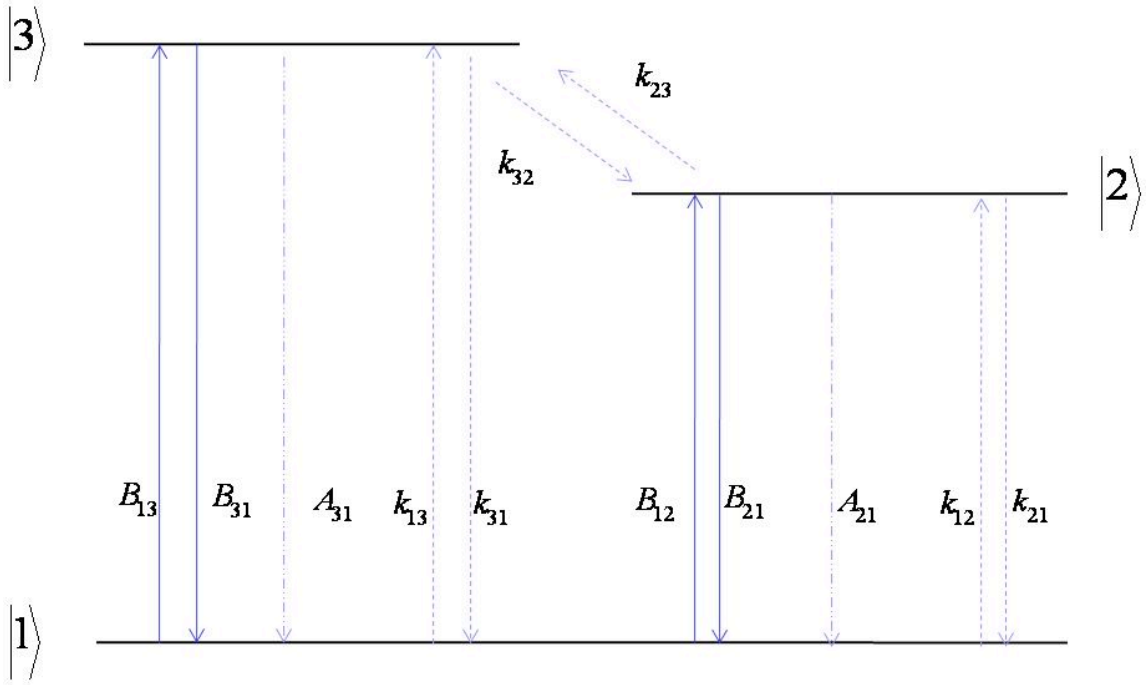

Figure 7. General Three Level System Diagram

Suppose we have a three level atomic system, as in Figure 7, where the first and third and the first and second levels are coupled by a dipole allowed transition. Next, the question can be asked what are the transition rates associated with the allowed transitions from TDPT. Incorporated in these transition rates are optical constants known as the Einstein A, B coefficients that have both classical and quantum mechanical interpretations.

Einstein A,B Coefficients

In order for a transition to take place from the first to the third level (or the first to the second) a radiation field must be present. Obviously this radiation field will not be composed of one solitary frequency matched to the energy difference of transition, but rather will have a distribution of frequencies which can be described by a Plank radiation distribution :

$$\rho(\omega) = \frac{\omega^2}{\pi^2 c^3} \cdot \frac{\hbar\omega}{e^{\hbar\omega/kT} - 1} \tag{1.66}$$

The rate at which atoms in the first level are promoted to the third level can be written down as:

$$R_{13} = N_1 B_{13} \rho(\omega) \tag{1.67}$$

where N_1 is the number density of atoms in the first energy level and B_{13} is known as the Einstein B coefficient which has units of $m^3\omega / Et$. Absorption isn't the only process occurring however. An excited atom in the third state can do one of two things. Spontaneously emit its absorbed energy in any direction or it can emit stimulated radiation by means of a dipole relaxation transition. This allows us to write down a rate equation for transition from the third level to the first:

$$R_{31} = N_3 B_{31} \rho(\omega) + N_3 A_{31} \tag{1.68}$$

where the A coefficient is in units of inverse seconds and a property of the atom itself. When the system comes to equilibrium we can take advantage of the Boltzmann distribution of population levels to write down the following relation:

$$\frac{N_3}{N_1} = \frac{g_3}{g_1} \cdot e^{-\hbar\omega/kT} = \frac{B_{13}\rho(\omega)}{B_{31}\rho(\omega) + A_{31}} \tag{1.69}$$

Solving for the radiation field we find a relation between the Einstein coefficients and the electromagnetic field present:

$$\rho(\omega) = \frac{A_{31}/B_{31}}{\frac{g_1}{g_3}\frac{B_{13}}{B_{31}} e^{\hbar\omega/kT} - 1} = \frac{\hbar\omega^3}{\pi^2 c^3} \cdot \frac{1}{e^{\hbar\omega/kT} - 1} \tag{1.70}$$

So the only way this can be true is if the A,B coefficients have the following relationships:

$$\begin{aligned} B_{13} &= B_{31}(g_3/g_1) \\ A_{31} &= \frac{\hbar\omega^3}{\pi^2 c^3} B_{31} \end{aligned} \tag{1.71}$$

The B coefficient can also be understood from a quantum mechanical point of view as well by starting with equation 1.56. Once again we wait a "long time" so that the system can come to equilibrium and write the TDPT coefficient as:

$$\begin{aligned} b_f^{(1)}(t) &= \lim_{T\to\infty} \frac{-i}{\hbar} \left\langle f^0 \left| \hat{\mathbf{H}}_1 \right| i^0 \right\rangle \int_{-T/2}^{T/2} e^{i\left(\omega_{f\,i} - \omega\right)t'} dt' \\ &= \frac{-2\pi i}{\hbar} \left\langle f^0 \left| \hat{\mathbf{H}}_1 \right| i^0 \right\rangle \delta(\omega_{f\,i} - \omega) \end{aligned} \tag{1.72}$$

Squaring this quantity we get the transition probability:

$$P_{i\to f} = \frac{4\pi^2}{\hbar^2}\left|\left\langle f^0 \left| \widehat{\mathbf{H}}_1 \right| i^0 \right\rangle\right|^2 \delta(\omega_{fi} - \omega)\delta(\omega_{fi} - \omega) \tag{1.73}$$

The double delta function encountered can be handled in the following way:

$$\begin{aligned} \delta\delta &= \lim_{T\to\infty} \delta(\omega_{fi} - \omega)\frac{1}{2\pi}\int_{-T/2}^{T/2} e^{i(\omega_{fi}-\omega)t}dt \\ &= \delta(\omega_{fi} - \omega)\lim_{T\to\infty}\frac{T}{2\pi} \end{aligned} \tag{1.74}$$

Now all that is left to do to derive the average transition rate is to substitute 1.74 into 1.73 and divide by T:

$$R_{i\to f} = \frac{2\pi}{\hbar}\left|\left\langle f^0 \left| \widehat{\mathbf{H}}_1 \right| i^0 \right\rangle\right|^2 \delta(E_f^0 - E_i^0 - h\nu) \tag{1.75}$$

If our initial and final states correspond to the first and third level of our three level system and recognizing that in equation 1.67 the quantity $B_{13}\rho(\omega)$ is also a rate we see that the B coefficient expressed through TDPT is:

$$B_{13} = \frac{\frac{2\pi}{\hbar}\left|\left\langle 3 \left| \widehat{\mathbf{H}}_1 \right| 1 \right\rangle\right|^2 \delta(\Delta E_0 - \hbar\omega)}{\rho(\omega)} \tag{1.76}$$

The same analysis can be done for the dipole transition between states 1 and 2 which will be fully expounded later in the paper for the full rate equation analysis.

Kinetic Considerations

Stimulated emission and absorption along with spontaneous emission are not the only process occurring in a three level system. If there exist foreign species in the system in a gaseous state, for instance hydrogen or methane, they will impart energy upon the atomic species in the form of collisions. What these collisions do to the states of the atom depend chiefly on two things, the energy of the colliding species and how well the foreign species can absorb energy in terms of rotational and vibrational excitations. How well a species can couple to the atomic species is beyond the scope of this research however the results are of utmost importance. Suffice to say a foreign species can do the following:

1) Promote an atom from state 1 to state 2 or 3.
2) Demote and excited atom from 3 or 2 down to 1.
3) Regulate the excited population states.

Each species will have its own ‘k’ coefficient and its affect on the population levels will depend on how much foreign species is present in the form of partial pressure, M. These kinetic factors will affect each population rate by the following functional form:

$$N_i \sum_x M_x \cdot k_{ijx} \tag{1.77}$$

where, x represents a foreign species and i,j represents different energy levels. Figure 1 depicts the three sets of kinetic interactions. The most important set is what are deemed the spin-orbit coefficients, k_{23} and k_{32}. These coefficients regulate how quickly population is de-excited from the third to second level. Table 4 lists the spin orbit coefficient k_{32} of Cesium and Rubidium between both Helium and Ethane.

Table 4. Rubidium and Cesium Spin Orbit k_{32} Constants

Collision Partners	Value (s^{-1}·$torr^{-1}$)
Cs-He	157.601
Cs-Ethane	$9.061 \cdot 10^{6}$
Rb-He	40137.500
Rb-Ethane	$1.082 \cdot 10^{7}$

Absorption Cross Section

In equation 1.75 the delta function dictates that a transition will only take place at a frequency equal to the difference of the transition energy levels. On the outset it seems that only one frequency will promote a transition, but this is not entirely true. Just as in blackbody radiation we find a spectrum of frequencies peaked at a certain value, there is also a spectrum of frequencies that can be absorbed by a stimulated response peaked at $E_f - E_i$. What modifies this absorption profile are deviations of an atom from its quantum mechanically defined energy level. These deviations come in the form of natural, thermal, and pressure deviations that tend to broaden the frequencies of radiation which would promote an atom.

The defining equation that entails all of this information will be termed the differential absorption law:

$$\frac{1}{I(\omega)}\frac{dI(\omega)}{dx} = -\Delta N \cdot \sigma_0 \cdot g(\omega) \tag{1.78}$$

where ΔN is the population inversion of the absorption manifold. Typically given in units of cm^2 is the integrated cross section σ_0 and is modified in frequency space by $g(\omega)$ or the lineshape of absorption. The lineshape function will capture all the effects that broaden the absorption profile.

Integrated Cross Section

The cross section can be thought of as a measure proportional to how much radiation is absorbed by an ensemble of atoms at a particular frequency. A relation can be made between the B coefficient and the cross section. The total rate at which photons are absorbed due to a stimulated response in the range of ω to ω + dω is:

$$R_{13}d\omega = B_{13}g(\omega)\rho(\omega)(N_1 - \frac{g_1}{g_3}N_3)d\omega \tag{1.79}$$

Multiplying this rate by $\hbar\omega$ and supposing that the power density is due to a beam of cross-sectional area A we find the power lost due to absorption as:

$$-\Delta P = \hbar\omega B_{13}g(\omega)\rho(\omega)(N_1 - \frac{g_1}{g_3}N_3)Ad\omega\Delta x \tag{1.80}$$

where Δx is simply how far the beam propagates. Dividing both sides of equation 1.80 and noting that $I(\omega) = \rho(\omega)c$ we find that:

$$\frac{\Delta P}{A\Delta x d\omega} \rightarrow \frac{dI(\omega)}{dx}$$

$$\frac{1}{I(\omega)}\frac{dI(\omega)}{dx} = -\hbar\omega B_{13} g(\omega)(N_1 - \frac{g_1}{g_3} N_3)/c \tag{1.81}$$

Comparing equations 1.81 with the differential law of absorption, equation 1.78, and using the relationship between the A, B coefficients in equation 1.71 we can calculate the integrated cross section from simply knowing the radiative lifetime:

$$\sigma_0 = \frac{\pi^2 c^2}{\omega^2}\frac{g_3}{g_1} A_{31} \tag{1.82}$$

Natural Broadening

Let us assume that for a moment we only have a two level system with one atom in the upper level at a strictly defined energy. According to the uncertainty principle if this atom is indeed so energetically well defined the time it would exist in that state would be nearly infinite! But the fact of the matter is that atoms do radiate and so it must be that our energy levels aren't defined to the precision we have made them out to be. Luckily this has not affected our analysis to this point, but to proceed further we can no longer ignore Heisenberg's Uncertainty Principle. Tightly clustered around the upper level is a small spectrum of energy levels that an excited atom can exist in. Correspondingly there is a spectrum of energy levels about the lower state as well. Pictorially we can have a transition from the lower band of energies to the upper band of energies:

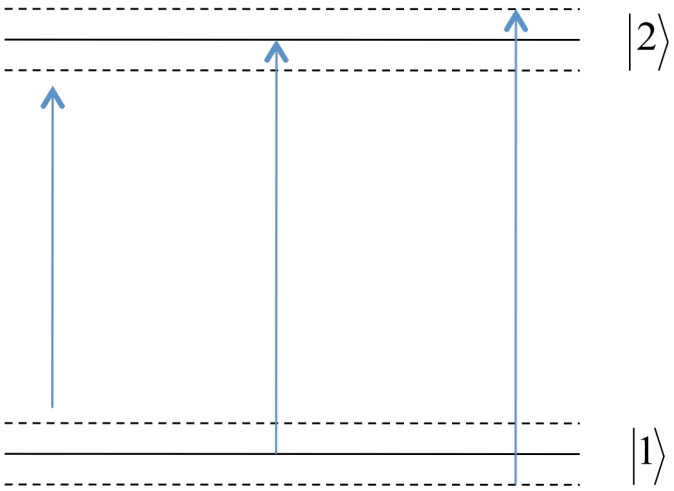

Figure 8. Effect of Uncertainty Principle on Energy Levels

Mathematically this distribution of absorption frequencies is Lorentzian in nature:

$$g(\nu-\nu_{21})=\frac{1}{2\pi}\cdot\frac{\delta\nu}{(\nu-\nu_{21})^2+(\delta\nu/2)^2} \tag{1.83}$$

where $\delta\nu$ is the Full Width Half Maximum (FWHM) and is equal to the A coefficient divided by 2π.

Doppler Broadening

Another phenomenon that will cause the absorption spectra to broaden as well is the Doppler effect. At a certain temperature the atoms to be excited will move with a certain kinetic energy dictated by a Maxwell Boltzmann distribution. Some fraction of the atoms in the system will therefore be moving parallel, anti-parallel, or some combination to the incoming electromagnetic wave. As such in the frame of the moving atom the imparted EM wave will be red or blue shifted accordingly. This shifting must then match an absorbing eigenfrequency if the atom is to be promoted. This leads to a

Gaussian distribution in the absorbing lineshape of the atoms with a corresponding FWHM dependent on temperature:

$$g(\nu-\nu_{21}) = \frac{2}{\delta\nu}\sqrt{\frac{\ln(2)}{\pi}}\cdot e^{-4\cdot\ln(2)[(\nu-\nu_{21})/\delta\nu]^2}$$
$$\delta\nu = 2\nu_{21}\sqrt{\frac{2kT\ln(2)}{mc^2}} \qquad (1.84)$$

Pressure Broadening and Pressure Shifting

The last observable fact that we will consider is pressure broadening, sometimes termed collisional broadening, and pressure shifting. A pure quantum mechanical treatment is very difficult to obtain for it depends on interatomic/intermolecular potentials between colliding parties. When two collisional partners are far apart their energy levels are that of their unperturbed state. However as they come within collision distances the potential surfaces of both the lower and upper level begin to change. The absorption frequency then becomes a function of intermolecular distance. The higher the pressure the more the atomic potential surfaces are effected which serves to broaden the frequency of absorption. Correspondingly high pressures can also totally shift where the transition frequency occurs by shifting both the upper and lower level unperturbed energy levels. Both the broadening coefficient and shifting coefficient depend on the particular collision partner. No closed form quantum mechanical derivation exists for such complicated potentials as such these parameters are experimentally measured and reported. For many cases it has been experimentally verified that a Lorentzian profile best approximates this effect:

$$g(\nu-\nu_{21}) = \frac{1}{2\pi}\cdot\frac{\delta\nu}{(\nu-(\nu_{21}+\Delta\nu))^2+(\delta\nu/2)^2}$$
$$\delta\nu = \sum_x b_x P_x \tag{1.85}$$
$$\Delta\nu = \sum_x b'_x P_x$$

where b is the broadening coefficient, b' is the shifting coefficient, and P is the pressure in torr of each separate collision species.

Complete Set of Rate Equations

Now one can write down the full dynamics of a three level atomic system in the presence of a stimulating radiation field and foreign collision partners as:

$$\begin{aligned}
\frac{dN_3}{dt} &= \frac{I_P(\nu)\sigma_{31}}{h\nu_P}(-N_3B_{31}+N_1B_{13}) - N_3A_{31} - N_3\cdot(\sum_x k_{31_x}M_x + \sum_x k_{32_x}M_x) \\
&\quad + N_2\cdot\sum_x k_{23_x}M_x + N_1\cdot\sum_x k_{13_x}M_x \\
\frac{dN_2}{dt} &= \frac{I_L(\nu)\sigma_{21}}{h\nu_L}(-N_2B_{21}+N_1B_{12}) - N_2A_{21} - N_2\cdot(\sum_x k_{21_x}M_x + \sum_x k_{23_x}M_x) \\
&\quad + N_3\cdot\sum_x k_{32_x}M_x + N_1\cdot\sum_x k_{12_x}M_x \\
\frac{dN_1}{dt} &= -\left(\frac{dN_2}{dt}+\frac{dN_3}{dt}\right)
\end{aligned} \tag{1.86}$$

Saturation Intensity

The saturation intensity is defined to be the intensity that decreases the absorption or gain to exactly half that of the small signal gain. The value of this intensity is particular for each system at specific system parameters for it depends on the cross section which is a function of frequency, temperature, and pressure.

$$I_s = \frac{\hbar\omega}{\sigma(\omega)} A_{31} \tag{1.87}$$

In fact equation 1.78 is a special case, known as the Beer's Law Limit, of the general differential absorption law. The general differential absorption law contains the saturation intensity as follows:

$$\frac{1}{I(\omega)} \frac{dI(\omega)}{dx} = \frac{-N \cdot \sigma_0 \cdot g(\omega) \cdot \alpha}{\beta + \chi \cdot \frac{I(\omega)}{I_s}} \tag{1.88}$$

with functions α, β, and χ determined from the specific system in question (See Appendix A). When the input intensity is far below the saturation intensity we recover equation 1.78. If the input intensity is far above the saturation intensity then the first term in the denominator of 1.88 can be ignored and we find linear behavior:

$$\frac{dI(\omega)}{dx} = \frac{-N \cdot I_s \cdot \sigma_{31} \cdot g(\omega) \cdot \alpha}{\chi} \tag{1.89}$$

Summary

With this background a comprehensive model can be pieced together to explore the various facets of what would affect a three level system when it is absorbing and lasing. The task at hand is to integrate all these separate phenomena and then check against experimental results to see the accuracy of the model. Once this is performed how important is one parameter over the other, or in other words how sensitive is the system to certain parameters, can be explored in the model rather than in experimental

laboratories. This model will also serve as a tool to help fine tune what a final DPAL system might look like.

II. Description of DPAL Absorption Model

Chapter Overview

This chapter describes how the absorption and lasing model of a three level DPAL system is constructed and controlled. The two alkalis modeled in this system are Rubidium and Cesium with the energy level diagram as seen below:

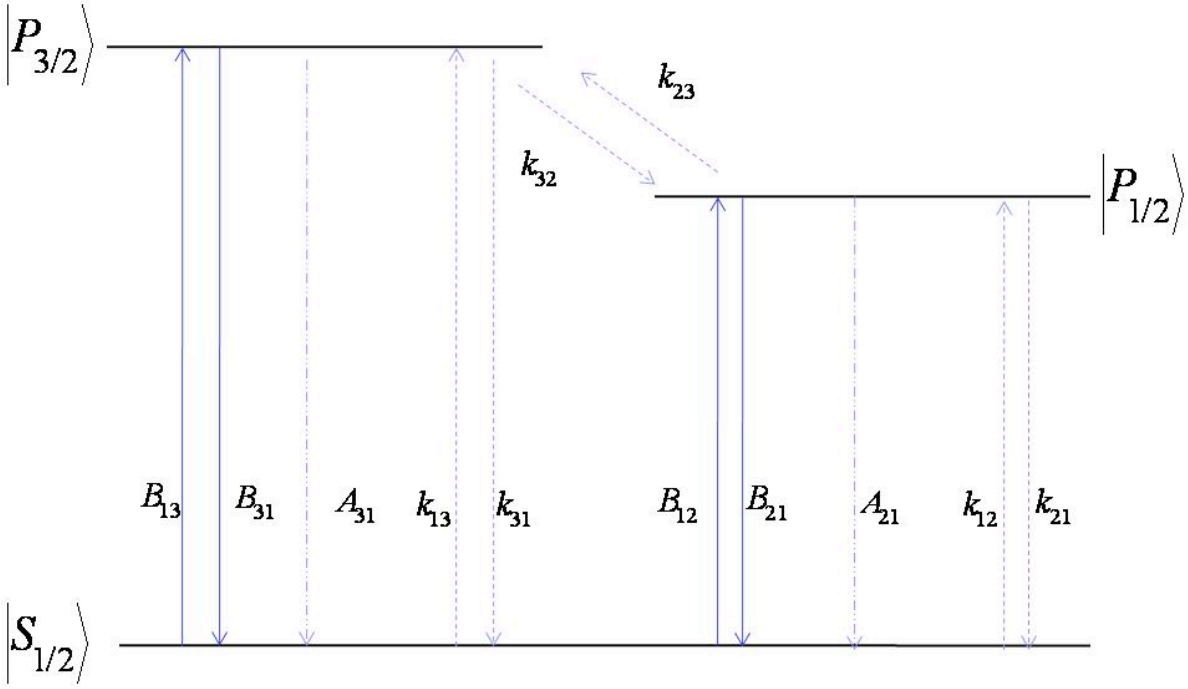

Figure 9. DPAL Three Level System Diagram

This model is completely written using Wolfram's Mathematica 6.0.1.0 32-bit version. This is a totally symbolic math package capable of solving and plotting user defined equations. The model first begins by the user defining the parameters of the system: temperature of the absorbing cell, temperature of the alkali cell, pressure of the foreign species (helium and ethane), power of the pump source, and finally the full width half-maximum of the pump source modeled as either a Gaussian or square wave. One

simply uses the control panel for absorption which consists of a set of “sliders” to pick what value one wishes for each parameter. Below is a picture of what the temperature parameter input sliders looks like.

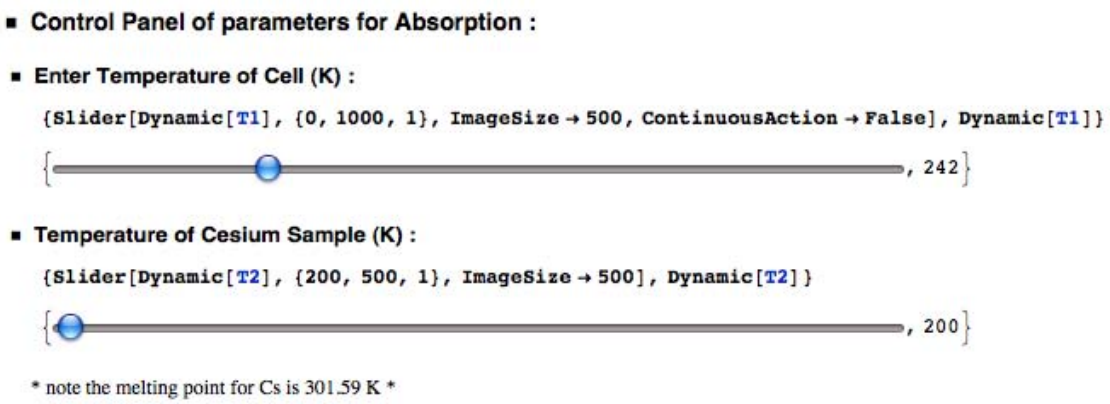

Figure 10. Parameter Control Panel

Once the parameters are set all that needs to be done is run the Mathematica kernel and the results are output at the end of the program code.

Constants and properties of the System

All physical constants are taken from the Committee on Data for Science and Technology’s (CODATA) recommendation list for fundamental physical constants dated 2006. The physical properties and optical constants of Rubidium and Cesium are taken from the experimental work of David A. Steck at the Los Alamos National Laboratory.

Computing Energy Levels and Transitions:

The first step to computing what frequencies will induce a transition is to first compute the available energy levels from quantum mechanics. Equations 1.4, 1.22, and 1.34 allow the calculation of energy levels to the hyperfine structure. Designate the

transition from the ground state, $6\ ^2S_{1/2}$, to the excited state , $6\,^2P_{1/2}$, the D1 transition manifold and from the ground state to the next higher excited state, $6\ ^2P_{3/2}$, the D2 transition manifold. Using the rules of the addition of angular momentum, in the case of Cesium, the ground state F value, where F equals the addition of electron spin, angular momentum, and nuclear spin, takes on 3 or 4. Then understanding equation 1.64, that is $\Delta F = 0, \pm 1$, we can calculate at what frequency to expect a hyperfine transition in both the D1 and D2 manifolds. Tables 5-7 predict these hyperfine transition frequencies. Note that in Tables 5-7 the transition frequency of the fine structure transitions or line center, $S_{1/2} \rightarrow P_{1/2}$ and $S_{1/2} \rightarrow P_{3/2}$, have been offset to zero. This is why there appears to be a negative transition frequencies.

Table 5. Cesium Transition Frequencies

D1 Manifold		D2 Manifold	
Transition (Gnd → Excited)	Frequency (MHz)	Transition (Gnd → Excited)	Frequency (MHz)
3→3	4514.04	3→2	4829.68
3→4	5681.72	3→3	4984.81
4→3	- 4678.60	3→4	5182.19
4→4	- 3510.92	4→3	- 4207.82
		4→4	- 4010.44
		4→5	- 3757.58

Table 6. Rubidium 85 Transition Frequencies

D1 Manifold		D2 Manifold	
Transition (Gnd → Excited)	Frequency (MHz)	Transition (Gnd → Excited)	Frequency (MHz)
2→2	1559.92	2→1	1657.64
2→3	1921.5	2→2	1687.01
3→2	-1475.81	2→3	1750.41
3→3	-1114.23	3→2	-1348.72
		3→3	-1285.32
		3→4	-1164.68

Table 7. Rubidium 87 Transition Frequencies

D1 Manifold		D2 Manifold	
Transition (Gnd → Excited)	Frequency (MHz)	Transition (Gnd → Excited)	Frequency (MHz)
1→1	3761.27	1→0	3969.6
1→2	4577.92	1→1	4041.82
2→1	-3073.42	1→2	4198.77
2→2	-2256.76	2→1	-2792.86
		2→2	-2635.92
		2→3	-2369.27

Computing Lineshapes

If the frequencies computed for the hyperfine transitions of the D1 and D2 manifolds are plotted we would produce what is known as a stick spectrum. As discussed earlier in this paper we have to account for three phenomena that would broaden this stick spectrum: natural, Doppler, and pressure. Not only that we also know that each transition has a certain strength calculated from the matrix elements via TDPT. In order to do this we form what is known as the Voigt profile. This is simply the convolution of a Gaussian with Lorentzian. The formed used of the Voigt profile in this model is as follows:

$$V(\nu,\nu_t)=\frac{\mathrm{Re}[e^{-z(\nu,\nu_t)^2}\cdot Erf(c-iz(\nu,\nu_t))]}{\frac{\delta\nu D}{\sqrt{8\log(2)}}\sqrt{2\pi}} \tag{1.90}$$

$$z(\nu,\nu_t)=\frac{\left(\nu-\nu_t+\delta He\cdot PHe\left(\frac{T}{294.15}\right)^{1/2}+\delta Me\ PMe\left(\frac{T}{294.15}\right)^{1/2}\right)+i\frac{\delta\nu L}{2}}{\frac{\delta\nu D}{\sqrt{8\log(2)}}\sqrt{2}} \tag{1.91}$$

where the full width half max of the Gaussian and Lorentzian profiles are:

$$\delta\nu D = (\nu_t + \nu_{\text{D1 or D2}}) \cdot \left(\frac{8kTLog(2)}{m_{Cs} \cdot c^2} \right)^{1/2}$$
$$\delta\nu L = \left(\frac{A}{2\pi} + \gamma He \cdot PHe \left(\frac{T}{294.15} \right)^{1/2} + \gamma Me \ PMe \left(\frac{T}{294.15} \right)^{1/2} \right) \quad (1.92)$$

Each hyperfine transition, ν_t, will be broadened according to equations 1.90-1.92. The summation of all transitions in a particular manifold will be the lineshape function $g(\nu)$. Each transition is further modified by the strength of transition, Table 8-10, and the relative population of the hyperfine split ground state based upon a Boltzmann distribution.

$$g(\nu) = \sum_t \frac{N_t}{N} S_t \cdot V(\nu, \nu_t) \quad (1.93)$$

Table 8. Relative Strength of Transition for Cesium

D1 Manifold		D2 Manifold	
Transition (Gnd → Excited)	Relative Strength (S_t)	Transition (Gnd → Excited)	Relative Strength (S_t)
3→3	1/4	3→2	5/14
3→4	3/4	3→3	3/8
4→3	7/12	3→4	15/56
4→4	5/12	4→3	7/72
		4→4	7/24
		4→5	11/18

Table 9. Relative Strength of Transition for Rubidium 85

D1 Manifold		D2 Manifold	
Transition (Gnd → Excited)	Relative Strength (S_t)	Transition (Gnd → Excited)	Relative Strength (S_t)
1→1	1/6	1→0	1/6
1→2	5/6	1→1	5/12
2→1	1/2	1→2	5/12
2→2	1/2	2→1	1/20
		2→2	1/4
		2→3	7/10

Table 10. Relative Strength of Transition for Rubidium 87

D1 Manifold		D2 Manifold	
Transition (Gnd → Excited)	Relative Strength (S_t)	Transition (Gnd → Excited)	Relative Strength (S_t)
1→1	1/6	1→0	1/6
1→2	5/6	1→1	5/12
2→1	1/2	1→2	5/12
2→2	1/2	2→1	1/20
		2→2	1/4
		2→3	7/10

Table 11. Broadening and Shifting Coefficients for Cesium

D1 Manifold		D2 Manifold	
Species	Broadening Coefficient (MHz/torr)	Species	Shifting Coefficient (MHz/torr)
γHe	26.21	γHe	23.50
γMe	29.1	γMe	26.2
δHe	4.46	δHe	0.75
δMe	-7.92	δMe	-7.00

(No experimental values exist for Cs-Ethane, so Rb-Methane values are used instead)

Solving the Rate Equations and Absorption of Pump Intensity

The form of the population inversion, $N_3 - (g_3/g_1)N_1$, is needed to understand how pump intensity is absorbed or attenuated through the absorption cell.. Assuming that the input laser is impingent upon the cell of alkali for a time much longer than any lifetime of

the system a steady state regime can be used to solve the rate equations. The rate equations then give how the population density numbers of each level change with respect to system parameters. First, set equations 1.86 such that dN/dt=0, i,e, steady state conditions. Secondly, add the constraint, the total number of alkali atoms, N, do not change, into the system of equations. This is simply stated as $N_2 = N - N_1 - N_3$ and is substituted into the time rate of change of population N_3. Lastly, rearrange the equations in to a matrix/vector form such that the "vector" is comprised of the population densities. N_3. As such the matrix equation becomes:

$$\begin{pmatrix} -\frac{I_p\sigma_{31}}{h\nu_p} - \frac{1}{\tau_3} - k_{23} & 0 & k_{13} + \frac{I_p\sigma_{31}}{h\nu_p}\frac{g_3}{g_1} - k_{23} \\ k_{32} & -\frac{I_L\sigma_{21}}{h\nu_L} - \frac{1}{\tau_2} & k_{12} + \frac{I_L\sigma_{21}}{h\nu_L}\frac{g_2}{g_1} \\ -k_{32} + \frac{I_p\sigma_{31}}{h\nu_p} + \frac{1}{\tau_3} & -k_{23} + \frac{I_L\sigma_{21}}{h\nu_L} + \frac{1}{\tau_2} & -(k_{12}+k_{13}) - \frac{I_L\sigma_{21}}{h\nu_L}\frac{g_2}{g_1} - \frac{I_p\sigma_{31}}{h\nu_p}\frac{g_3}{g_1} \end{pmatrix} \begin{pmatrix} N_3 \\ N_2 \\ N_1 \end{pmatrix} = \begin{pmatrix} -Nk_{23} \\ 0 \\ 0 \end{pmatrix} \quad (1.94)$$

where the shorthand notation $k_{ij} = \sum_x M_x k_{ijx}$ is used for the spin orbit constants (reference equation 1.77). Using Kramer's Rule for a 3x3 matrix the vector in equation 1.95 can be solved for and the components of this vector are the quantities sought after (Appendix A).

Absorption Profiles

The absorption profile is derived from equation 1.78 and Mathematica will be used to plot the attenuation of the input pump as a function of frequency and distance into the absorbing cell. The population inversion used to solve equation 1.78 was derived

from solving equation 1.95. In computing population inversions the degeneracy of each state must be factored in as well. For the D2 manifold the inversion density is:

$$\Delta N = N_3 - \frac{g_3}{g_1} N_1 \tag{1.95}$$

Before solving equation 1.88 one of three scenarios can be chosen. First, absorption and lasing can be turned "off" by setting I_p and I_L equal to zero. This would say only kinetic processes. Second, setting I_L to zero would only allow for stimulated absorption and kinetic processes to run in the simulation. Lastly, by leaving the rate equations as is all processes are allowed to run. As the particular form of the solution will be slightly different based on what processes are allowed to run, the attenuation of the pump beam, using Mathematica's solver techniques, will have a functional form similar to the following:

$$I(x,\nu) = I_{sat}(\nu) \cdot \text{ProductLog}\left(\frac{e^{\frac{I_0}{I_{sat}} - \Delta N \cdot x \cdot \sigma_{31}(\nu)} \cdot I_0}{I_{sat}(\nu)} \right) \tag{1.96}$$

where I_0 is the input power set by the user in the parameter control sliders. This model uses both a Gaussian and square wave input profile which also has a user defined full width half maximum.

The Product Log, also known as the Lambert-W function, seeks to invert the equation $f(w) = we^w$ and solve for w. This complex transcendental function is not

injective and therefore will have more than one solution. However, since the parameters of the system are user defined, it will be obvious when a particular value of equation 1.97 is unphysical. When this happens Mathematica can be used to search for physical solutions.

Differential Transmittance

The last aspect that this model simulates is what is termed to be the differential transmittance. The differential transmittance is defined as the percent chance, that once steady state conditions have been established, a photon propagated through the entrance of the cell will be transmitted at a particular distance in to the cell. We say that the cell is transparent from the entrance of the cell to the distance at which the differential transmittance equals zero percent. Beyond this point the cell becomes totally opaque. The boundary between these two regions, transparency and opaqueness, is called the bleached wave front. As such saying a cell is completely bleached is equivalent to saying the cell is totally transparent. If a cell is not completely bleached then there exists a region in the cell that is opaque to incoming photons. This differential transmittance therefore is a visual representation of what a bleached wave looks like and can be used to determine how far a bleached wave penetrates a particular absorbing cell. The functional form of differential transmittance is derived from taking the derivative of equation 1.97 with respect to the initial pump intensity.

$$\frac{dI(x,\nu)}{dI_0(0,\nu)} = \text{dtransmittance}(x,\nu) \tag{1.97}$$

Summary

Using the principles put forth in the beginning of this paper this model simulates how an initial pump beam is attenuated through an absorbing cell of alkali vapor under a variety of adjustable system parameters. Every aspect of the model, energy levels, saturation intensities, lifetimes, etc. can be probed in detail to help understand what parameters the system is most sensitive to and which parameters have subtle of drastic effects on input attenuation. Also with such a detailed model analytic solutions derived by other means can be compared to see the efficacy of its assumptions.

III. Model Results

Chapter Overview

This chapter will focus on what type of outputs this DPAL absorption model can produce along with its comparisons to experimental results and analytical derivations. Also we can show how various features, like cross section and saturation intensities, change with change in system parameters. The focus of the results will center on two different regimes. The first will be akin to what we would see in a Beer's Law experiment: low power, low alkali concentration, and a low amount foreign species in the absorption cell. The second regime will be more of what would occur in a typical DPAL absorbing system: high input power and high Helium/Ethane pressure. Two general comparisons will be made as well. The first will be a comparison of this numerical model with an analytical quasi-two level analysis (QTLA) model. The second comparison will be how attenuation is affected in the presence of a lasing field solely within the quasi-two level regime. Table 11 contains the parameters that will be used for the two regimes discussed.

Table 12. Simulation Parameters

Parameter	Beer's Law Regime	DPAL/QTLA Regime
Temperature of Cell (K)	400	455
Alkali Concentration (#/volume)	6.7×10^{11}	6.1×10^{12}
He Pressure (torr)	50	200
Ethane Pressure (torr)	50	600
Input Peak Intensity (W/cm^2)	.60	200

Spectroscopic Comparison

Step by step analysis and comparison of this model must start from the beginning if the model is to be viable. The first step in this process is to simply compare experimental spectroscopic results with the lineshape of this model. From equation 1.78 we can write the solution as:

$$Ln\left(\frac{I}{I_0}\right) = -N \cdot L \cdot \sigma(\nu) \tag{1.98}$$

where L is the length of the cell. The right hand side of equation 1.99 is simulated and compared to a transmission experiment. The results are in Figure 11 below.

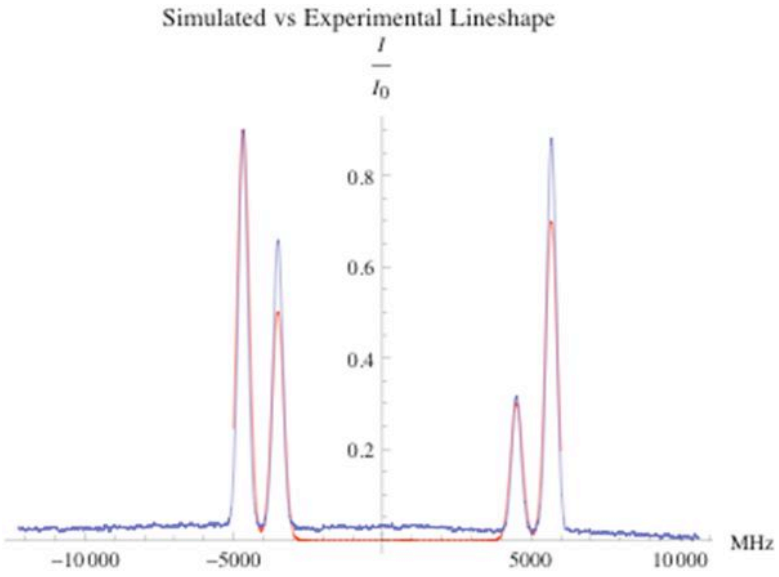

Figure 11. Simulated vs. Experimental Lineshape

Predicted Cross Sections and Pressure effects:

As discussed in the background section there are three main processes that lead to a broadening of the lineshape: natural, Doppler, and pressure broadening/shifting. Of the three pressure broadening/shifting has the most dramatic effect on line shape as captured

in Figures 12-17. As the pressure rises the hyperfine peaks begin to merge into one another. The cross section at line center rises until it reaches a maximum at slightly more than 600 torr of foreign gas species. At this point all hyperfine transition lines have blended and with the added pressure this value begins to descend again. Also that once the line shape has become one broad peak that the pinnacle of this peak is being shifted toward positive frequency in Figures 15-17. As the pressure keeps increasing the two trends, broadening and shifting, become more pronounced and more dominate. Natural and Doppler broadening are still accounted for, however the pressure effects, even when the pressure is low, tends to overshadow these two processes. In practice and in a real DPAL system pressure broadening will be the chief mechanism to broaden the cross section so that it matches the input shape of the pump.

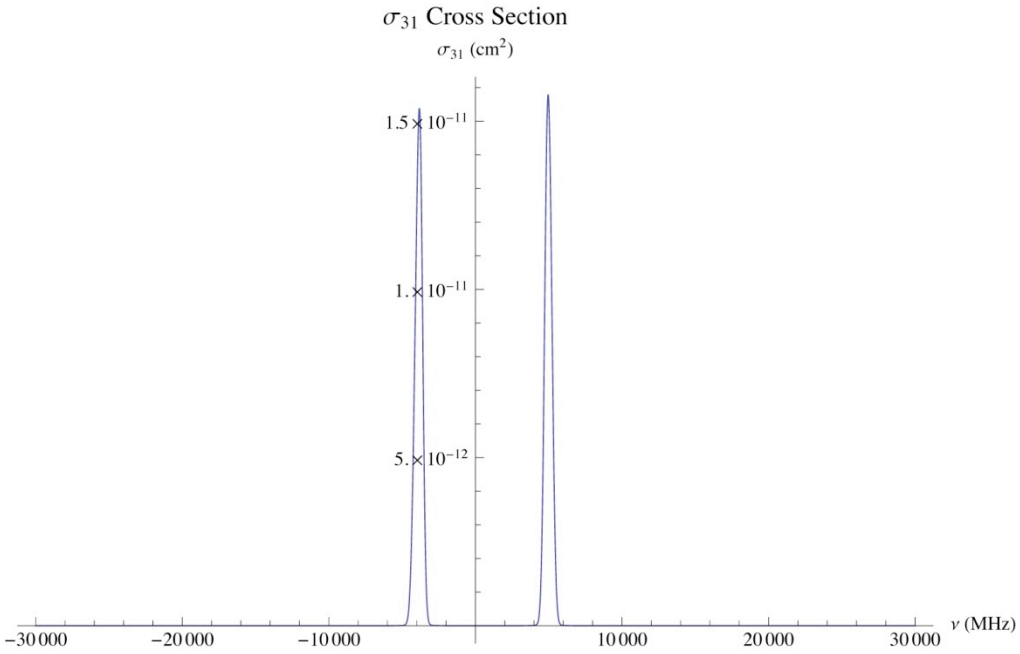

Figure 12. σ_{31} Cross Section at 0 torr He and 0 torr Me

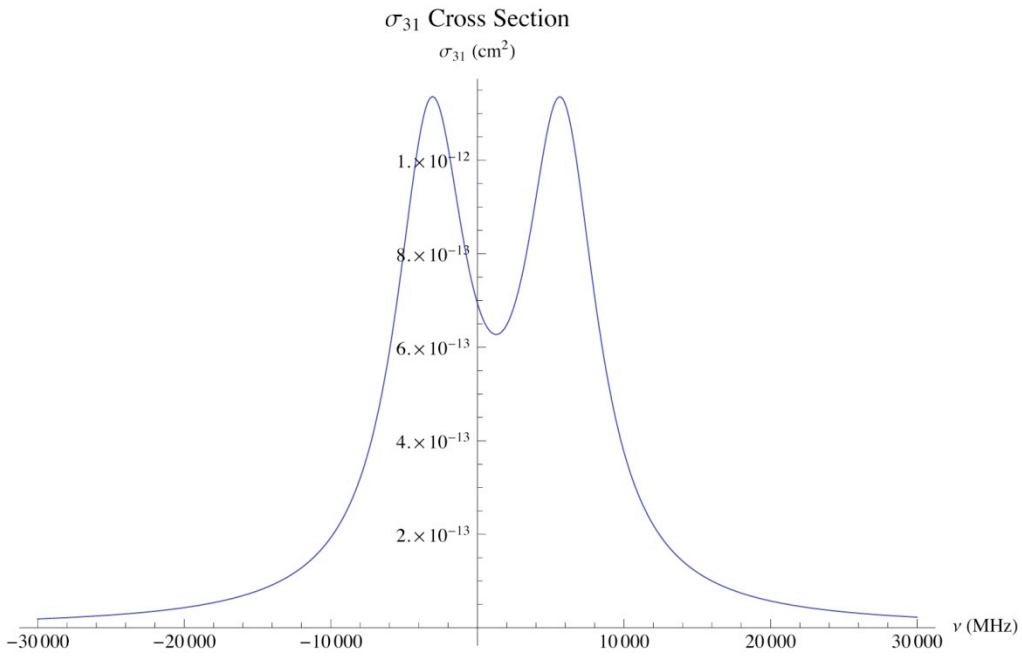

Figure 13. σ_{31} Cross Section at 100 torr He and 100 torr Me

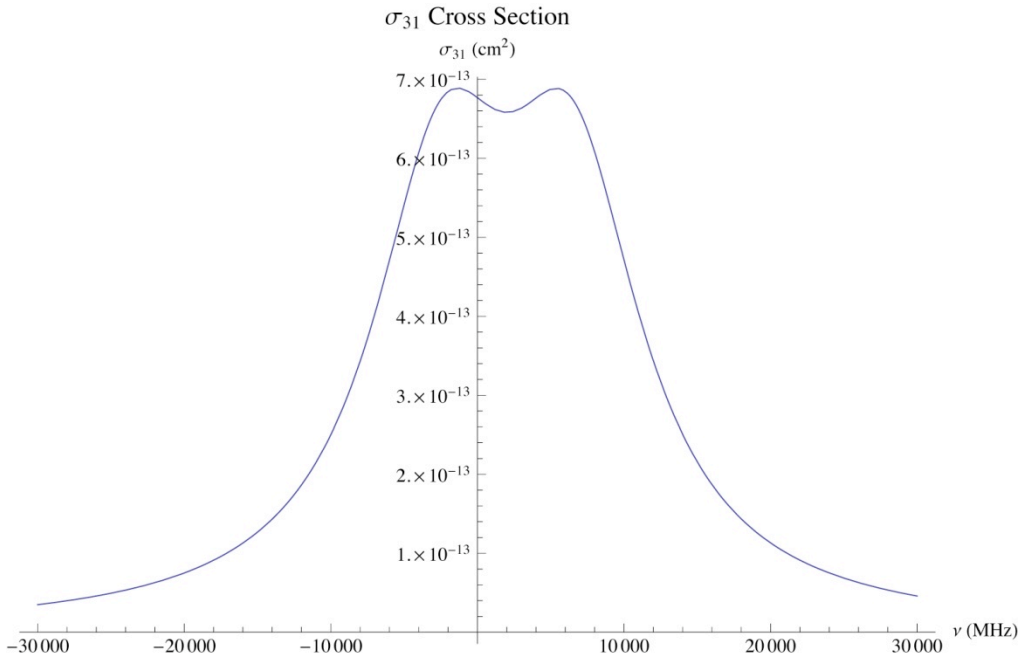

Figure 14. σ_{31} Cross Section at 200 torr He and 200 torr Me

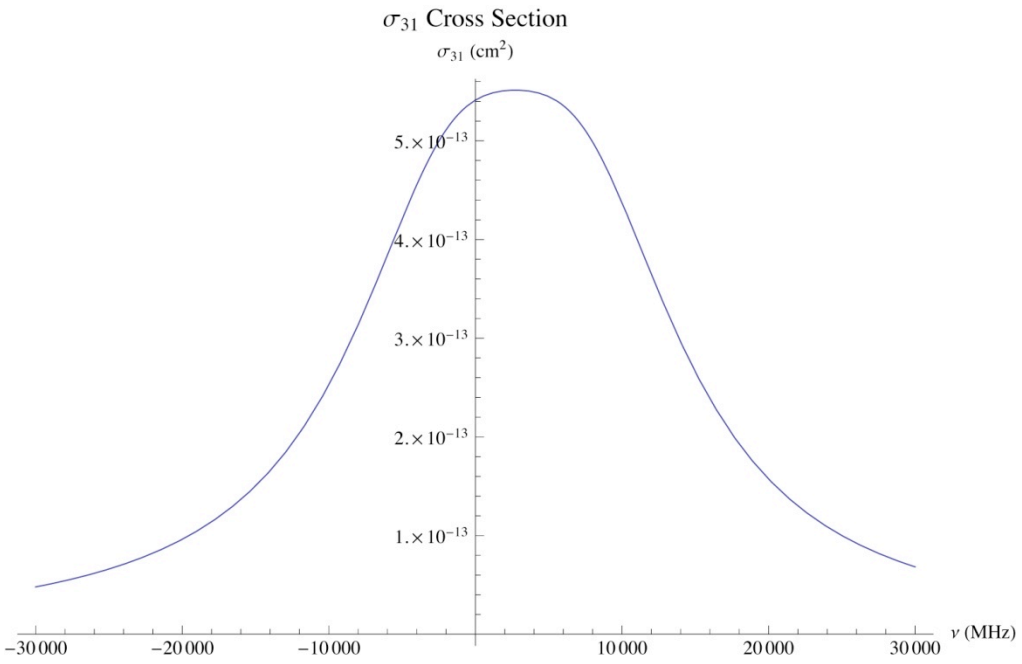

Figure 15. σ_{31} Cross Section at 300 torr He and 300 torr Me

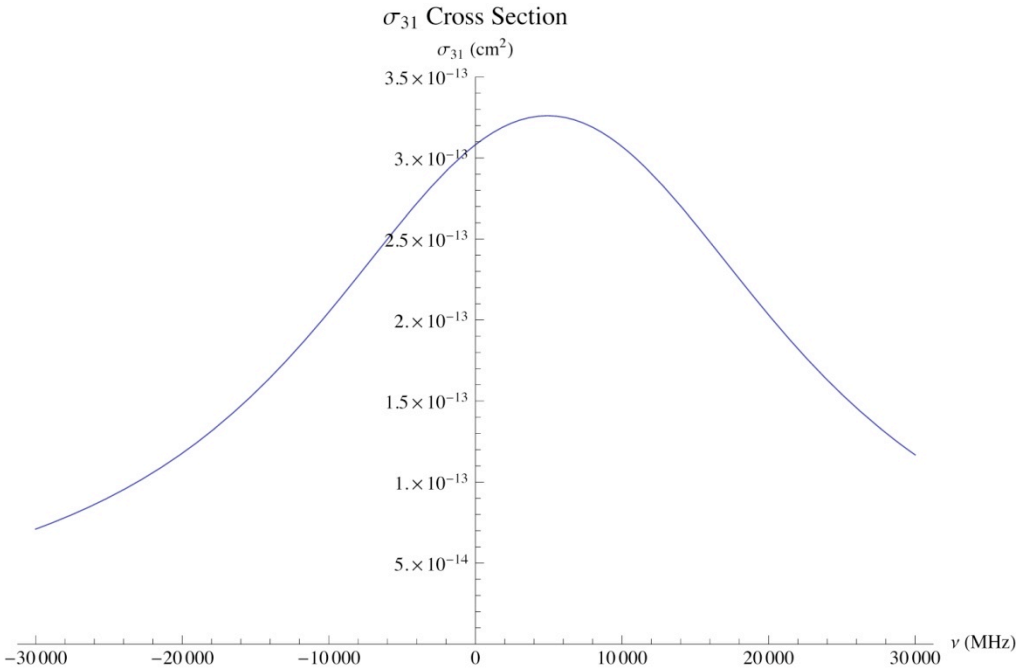

Figure 16. σ_{31} Cross Section at 600 torr He and 600 torr Me

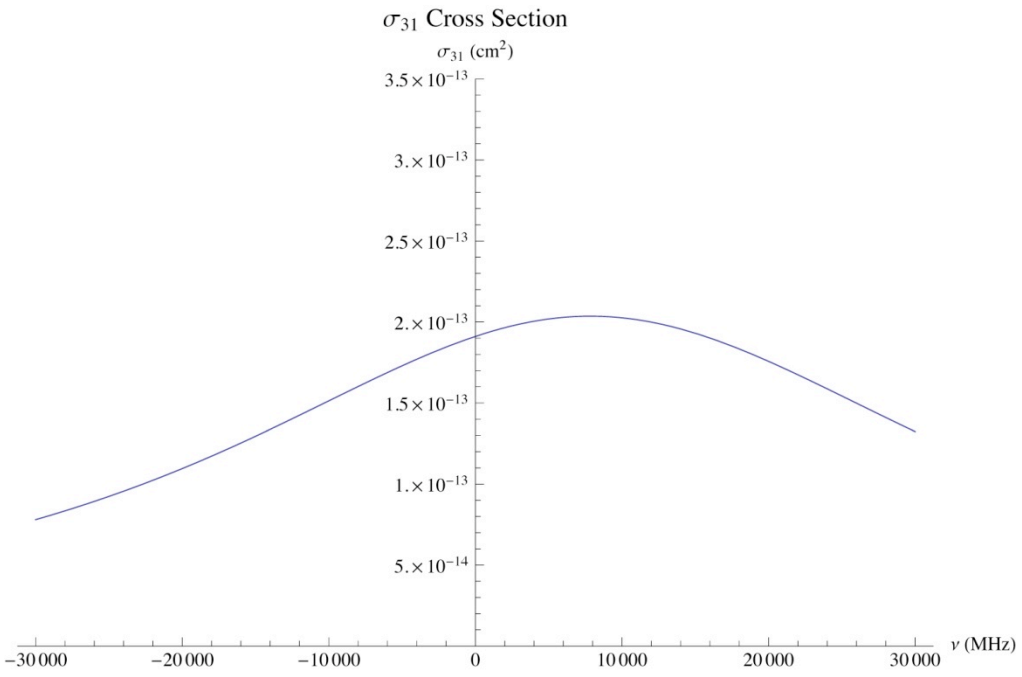

Figure 17. σ_{31} Cross Section at 1000 torr He and 1000 torr Me

Lifetimes and Saturation Intensities:

This model takes spectral look into the makeup of the saturation intensity. As described by equation 1.87 the spectral saturation intensity is inversely proportional to the lineshape. Just as the lineshape varies dramatically with pressure so does the spectral saturation intensity. The value of the saturation intensity is of utmost importance because of its relation to analytical forms and approximations as seen in the general differential absorption law. Three methods were employed to compute the value of the average saturation intensity from the spectral saturation intensity. The first was to take an average over a user defined frequency interval. The second method was to take the value of the spectral saturation intensity at each hyperfine transition (six for the D2 manifold) and simply average those values. Lastly, one can average over the lineshape (which is unity)

and simply use the value for the integrated cross section for equation 1.87. In the end the second method was used to compute the average saturation intensity. The first method can become cumbersome and computationally lengthy if too big a frequency interval is chosen. Also there is no clear delineation of where one should mark the beginning and the end of the frequency interval. The third method rids the saturation intensity of any dependence on system parameters and it simply becomes a constant. Method number 2 seems to be the most sensible and logical for it has two advantages: 1.) it takes into account pressure variations in the lifetime of the state and cross section and 2.) the six most important frequencies are undoubtedly accounted for and given importance. Figures 18 and 19 show plots of the spectral dependence of the saturation frequencies in both regimes and Table 13 displays calculated averages for all three methods.

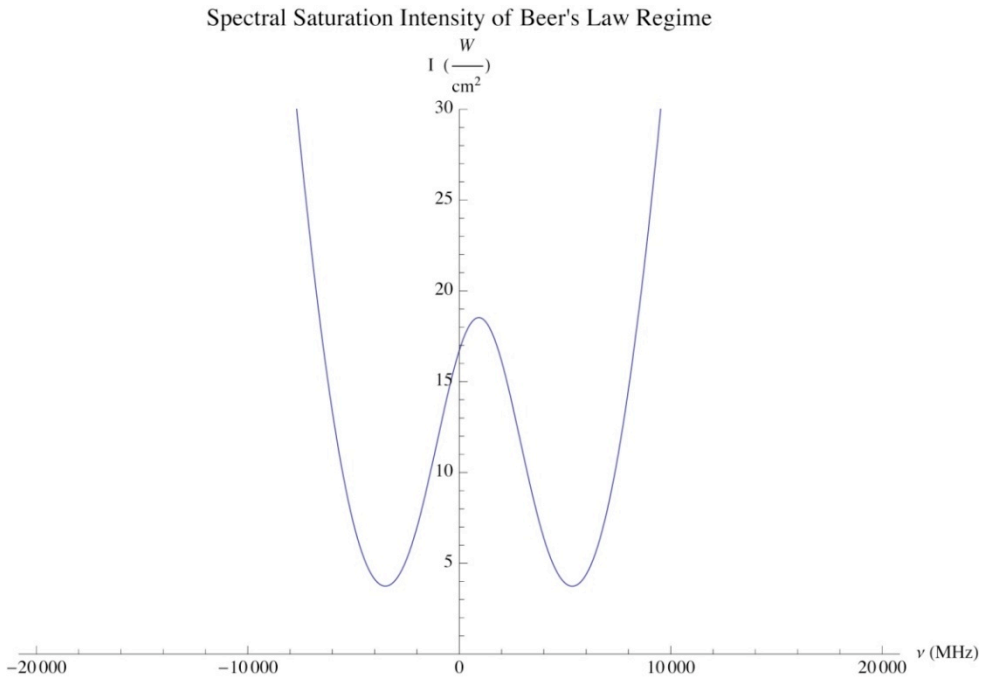

Figure 18. Spectral Saturation Intensity for Beer's Law Regime

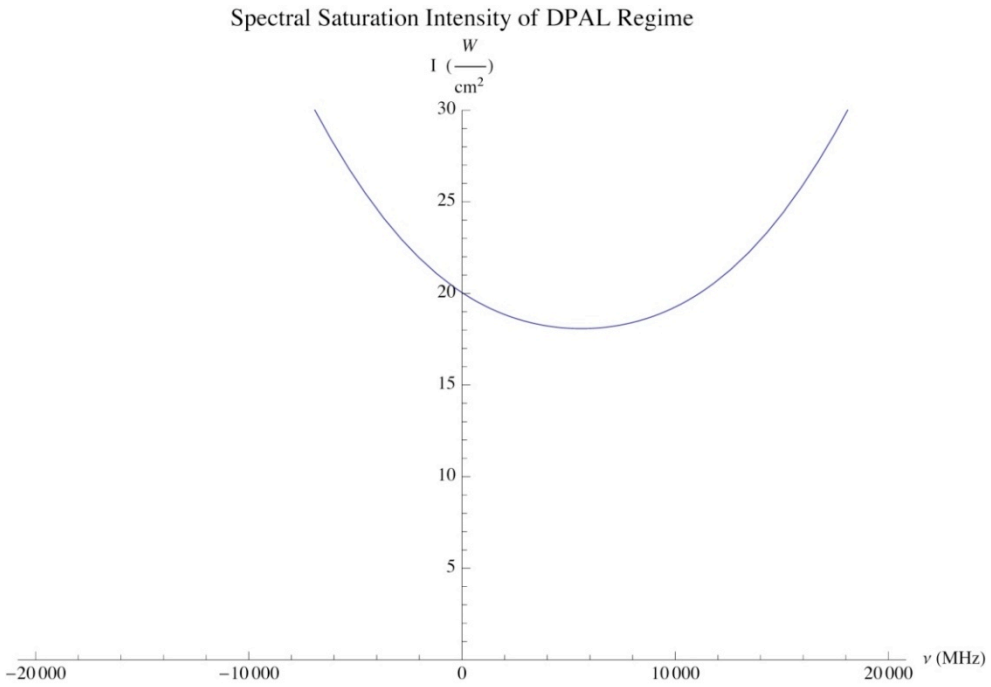

Figure. 19. Spectral Saturation Intensity for DPAL Regime

Table 13. Average Saturation Intensities

Isat (W/cm^2)	Method #1	Method #2	Method #3
Beer's Law Regime:	7.80	4.05	0.00040
DPAL Regime:	24.93	21.34	0.00040

Absorption Profiles

Rate Equation Population Inversions:

In order to solve equation 1.78 the population inversion is first calculated. Using equations 1.95 and 1.96 the population inversion for absorption is:

$$\Delta N_{31} = \frac{N(-2 + k_{13}\tau_3 + k_{23}k_{12}\tau_2\tau_3 + 2k_{32}k_{23}\tau_2\tau_3)}{(1 + k_{12}\tau_2 + (k_{13} + k_{23}(k_{12} - k_{32})\tau_2 + k_{13}k_{32}\tau_2)\tau_3) + \frac{I}{Isat}(3 + k_{12}\tau_2 + 2k_{32}\tau_2)A_{31}\tau_3} \quad (1.99)$$

Once equation 1.101 is substituted into 1.78 and all necessary functions and parameters are defined the solution for absorbed intensity can be explored in detail from a spatial and spectral perspective. As mentioned before when the input intensity is much greater than the saturation intensity linear behavior is expected. When below the saturation intensity exponential behavior is expected. The full solution is then a non-linear mixture of the two.

Frequency and spatial representation of Intensity

With equation 1.78 solved we first start with the Beer's Law regime and plot what the absorption profile looks like as a function of space and frequency. A square wave input pump with a FWHM of 20,000 MHz was used with a peak intensity of 0.60 Watts/cm^2. Noting that the saturation frequency for this regime was 4.05 Watts/cm^2 the input is well below the saturation value. Figure 20 displays the solution to equation 1.78.

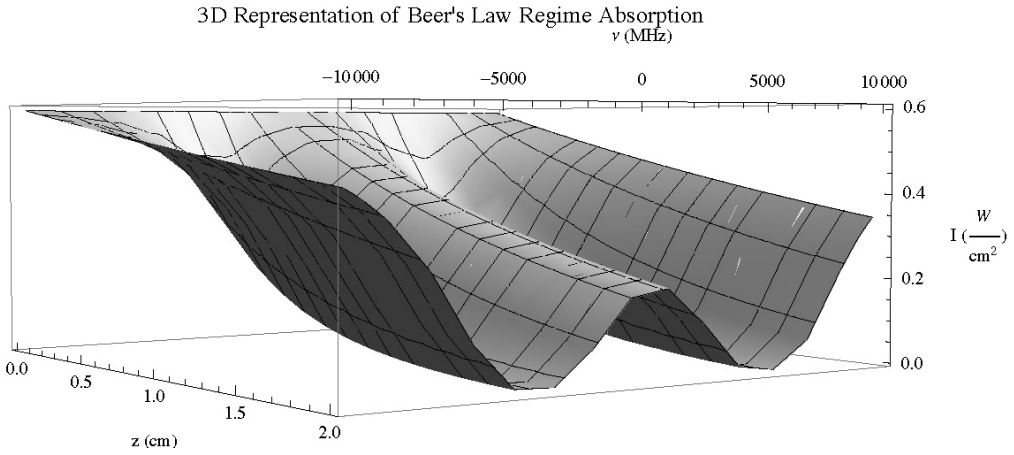

Figure 20. 3D Representation of Beer's Law Regime Absorption

With a pretty low system pressure the cross section is highly peaked around its hyperfine transitions. Also since the input is below the saturation frequency we would

expect the intensity to decay exponentially in space and be centered on the hyperfine peaks. Indeed this is what is captured in Figure 20. The two valleys do decay exponentially showing that all input power has been absorbed. Upon looking at Figure 20 one might also ask why there is no decay in between the hyperfine valleys since the saturation frequency is so high? The saturation frequency is inversely proportional to the cross section. So a low cross section means high saturation frequency. However in this case the cross section is so low between the valleys that hardly any absorption takes place. So the saturation intensity has no effect in this region. The region is therefore completely transparent. An electromagnetic wave with a bandwidth of around 7000 MHz centered about the fine transition frequency would simply transmit through. This window has an interesting feature in that its bandwidth can be completely controlled by the pressure of the system. Increasing the pressure would cause the bandwidth to decrease.

The plot for the DPAL regime looks different than the Beer's Law regime. With the system pressure being a total of 800 torr the hyperfine peaks have been broadened to the point where the cross section is one peak akin to Figure 15. The input pump for this simulation is a Gaussian with a FWHM of 20,000 MHz and a peak intensity of 200 W/cm^2. Being way above the saturation frequency linear behavior is expected. Figures 21 and 22 are the model results.

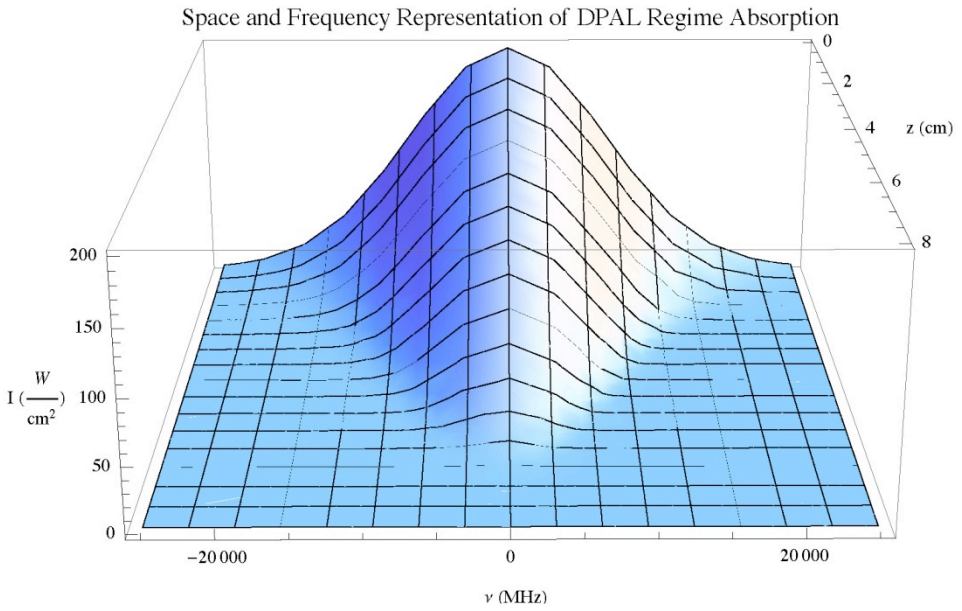

Figure 21. Space and Frequency Representation of DPAL Regime Absorption (Head on)

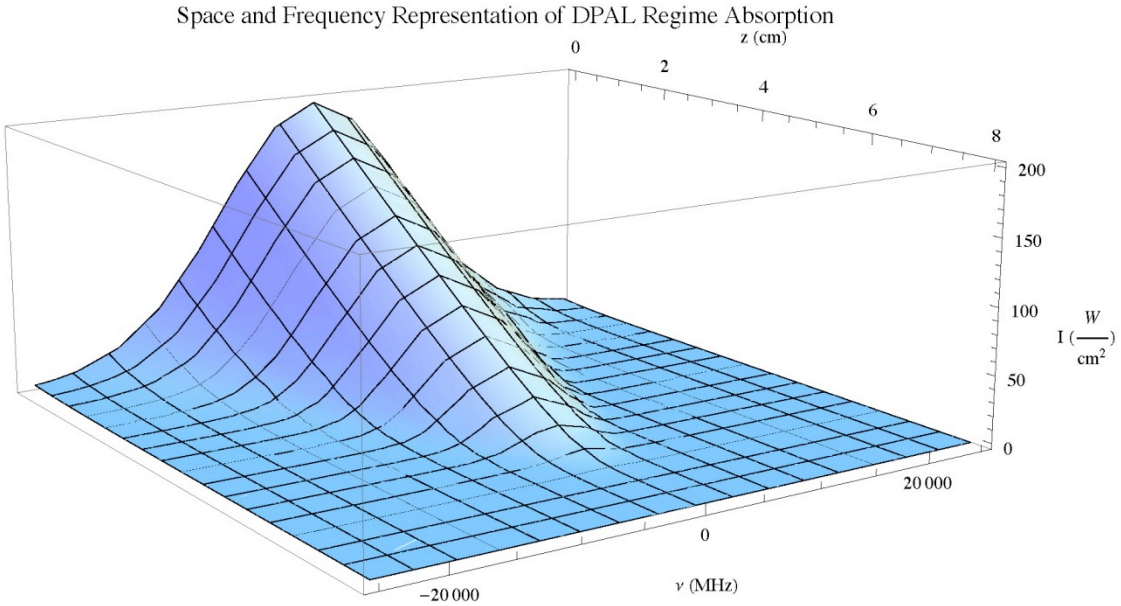

Figure 22. Absorption Profile DPAL Regime (3/4 View)

The input pump was matched pretty close in bandwidth to the cross section at 800 torr. At the entrance face (0 cm) of the cell the shape of the input pump is an obvious

Gaussian. As the power is absorbed a linear decay is observed at every frequency. Right before termination however the profile loses its linear dependence. This suggest that perhaps a linear approximation can be used to determine a cell length of a DPAL absorbing system. The linear nature of this region using equation 1.89 is:

$$I(x,\nu) = I_0(\nu) + \frac{2Nx\sigma_{31}(x,\nu)\, I_{sat}(x,\nu)\cdot(-1+k_{32}\,k_{23}\tau_2\tau_3)}{(3+2k_{32}\tau_2 A_{31}\tau_3)} \qquad (1.100)$$

From inspection of Figures 21 and 22 it's hard to discern when the profile ceases to be linear and how fast or slow it transitions from being linear to exponential. Eventually as intensity is absorbed throughout the cell at some point that intensity will be at or below saturation intensity and that is why the profile rolls off as it nears zero.

To see this more closely observe the profile at one frequency, in this case the 4 to 3 hyperfine transition, at various input powers of Isat plotted against the linear approximation. Figure 22 below shows such a plot. The four sets of curves shows are, starting from highest to lowest, input powers of 7, 5, 3, and 1 times of Isat labeled a, b, c, and d respectively. The trend is clear, the higher the initial pump intensity is compared to that of Isat, the more the absorption profile follows a linear trend. Even at seven times the saturation intensity the profile deviates from linear behavior rather quickly. At about ½ centimeter into the cell, exponential behavior begins to be mixed into with the linear behavior. It is obvious that the linear approximation fails to predict at what distance into the cell the input is attenuated to zero, by more than 50%, when the pump intensity starts near Isat.

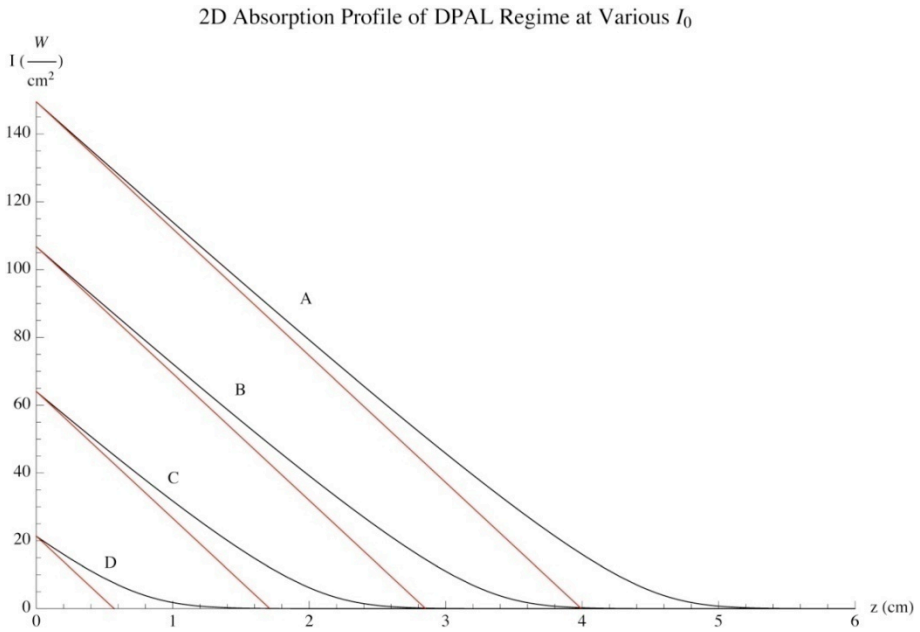

Figure 23. 2D Absorption Profiles of DPAL Regime at Various I_0.

Differential Transmittance and the Bleached Wave

As stated already another quantity can be explored using this model termed differential transmittance. This dTransmittance profile is produced by taking the derivative of the absorption profile with respect to the input pump. Such a profile will be able to tell us where, if added to the system after absorbing conditions have been established, one photon will leave the area of transparency and hit a saturation curtain at a particular frequency. The importance of such profile lies in the fact that if the laser is to operate at peak efficiency one must make sure that no saturation curtain exists in the cell. In essence this area of transparency is called a bleached wave and this dTransmittance profile is a visual representation of this wave.

The differential transmittance profile for the Beer's Law regime is rather uninteresting and is shown in Figure 23 along with its transmittance plot in Figure 24.

Once again in Figure 24 we see the transmission window a bandwidth of about 7000 MHz.

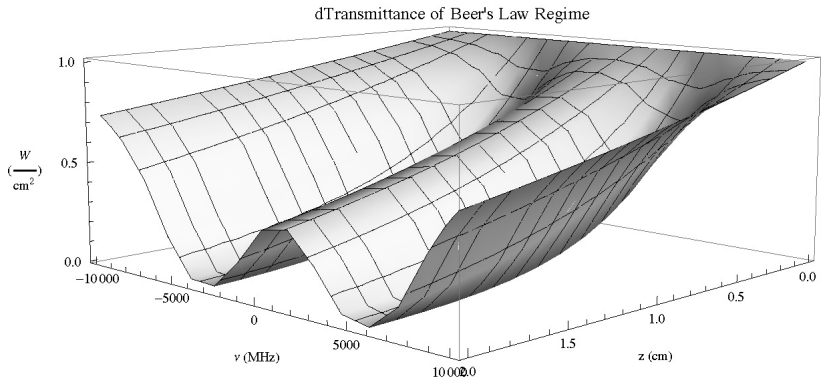

Figure 24. dTransmittance Profile Beer's Law Regime

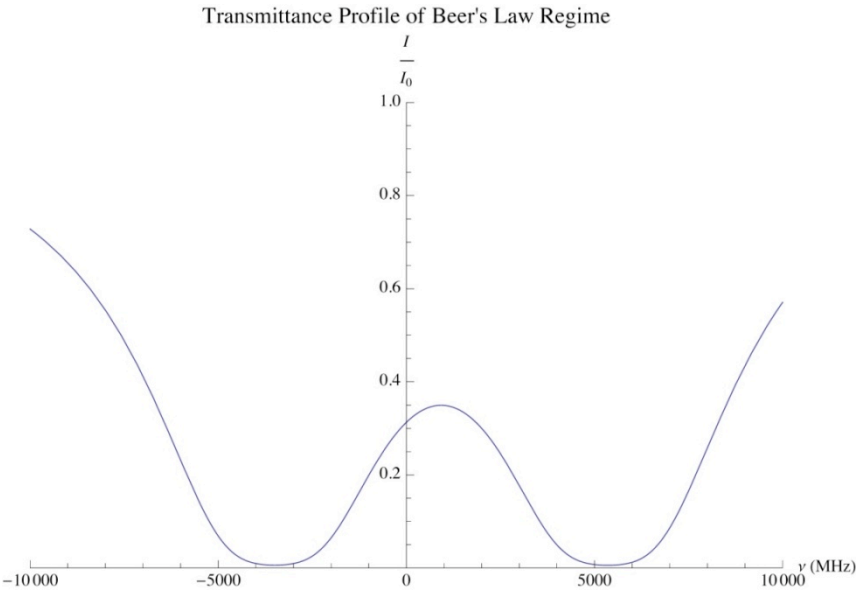

Figure 25. Transmittance Profile Beer's Law Regime

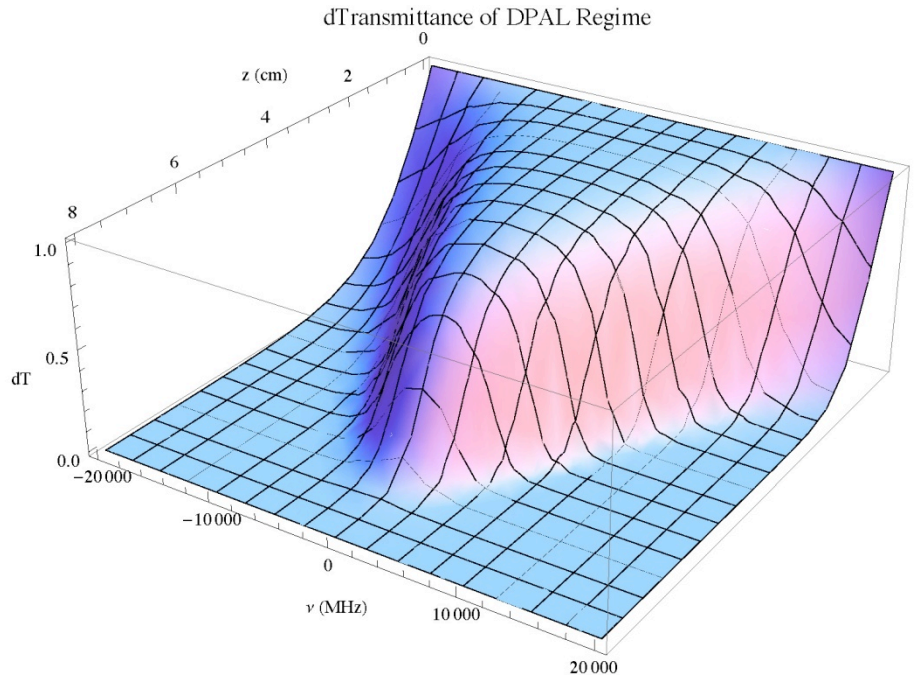

Figure 26. dTransmittance Profile DPAL Regime

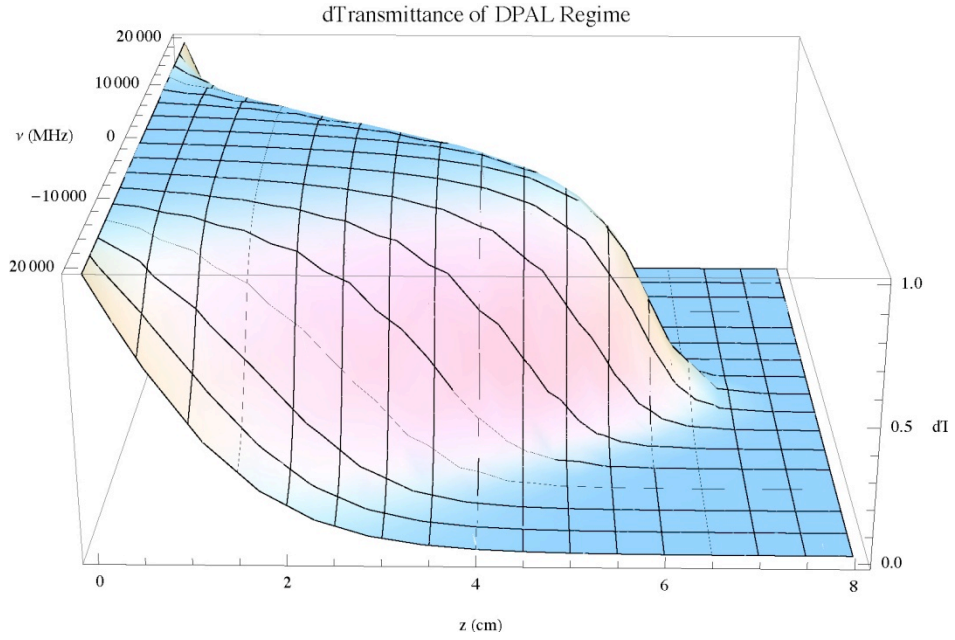

Figure 27. dTransmittance Profile DPAL Regime

The dTransmittance profiles for the DPAL regime are very revealing and are displayed in Figures 25 and 26. As one can see, after absorbing conditions are set, if one photon was

sent through the entrance of the cell that did not add any significant intensity to the pump it would travel unobstructed until it would hit an opaque. It is clear that this profile has an abrupt crash where the transparency/opaque interface occurs, hence the bleached wave nomenclature. In the case for these DPAL system parameters, in order to maximize absorption throughout the cell, the length would need to be around 6 cm in length.

This being an inherently numerical model the question arises is there any quick analytic determination to the length of the bleached wave? Turning to the linear approximation Figures 27 and 28 examine the performance of this approximation to bleached wave characteristics.

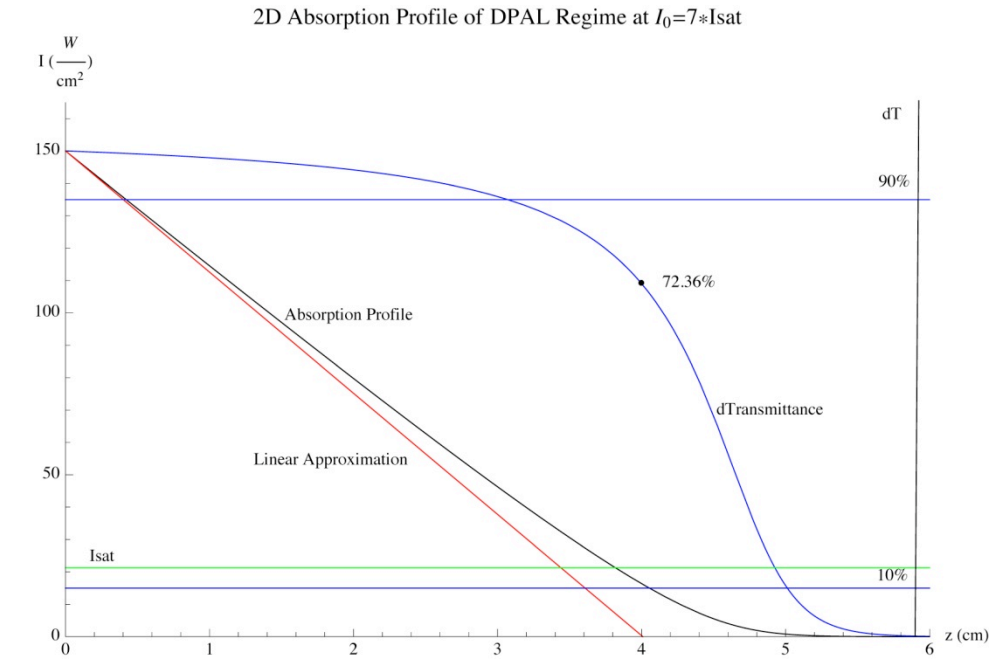

a.

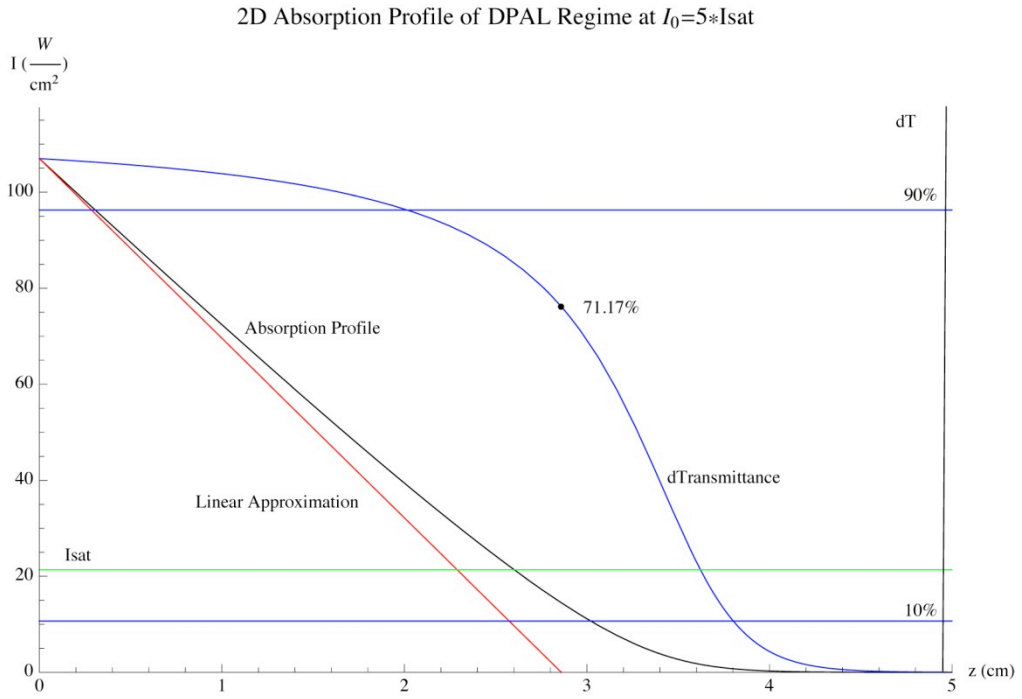

b.

Figure 28. Linear Approximation Performance at a.) 7xIsat and b.) 5xIsat

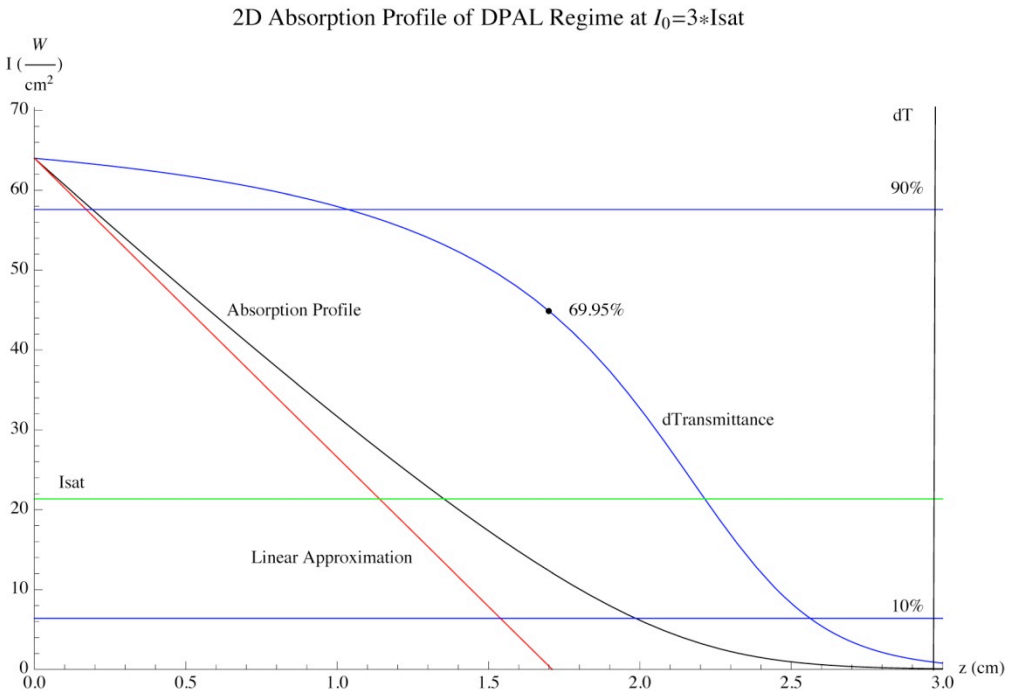

a.

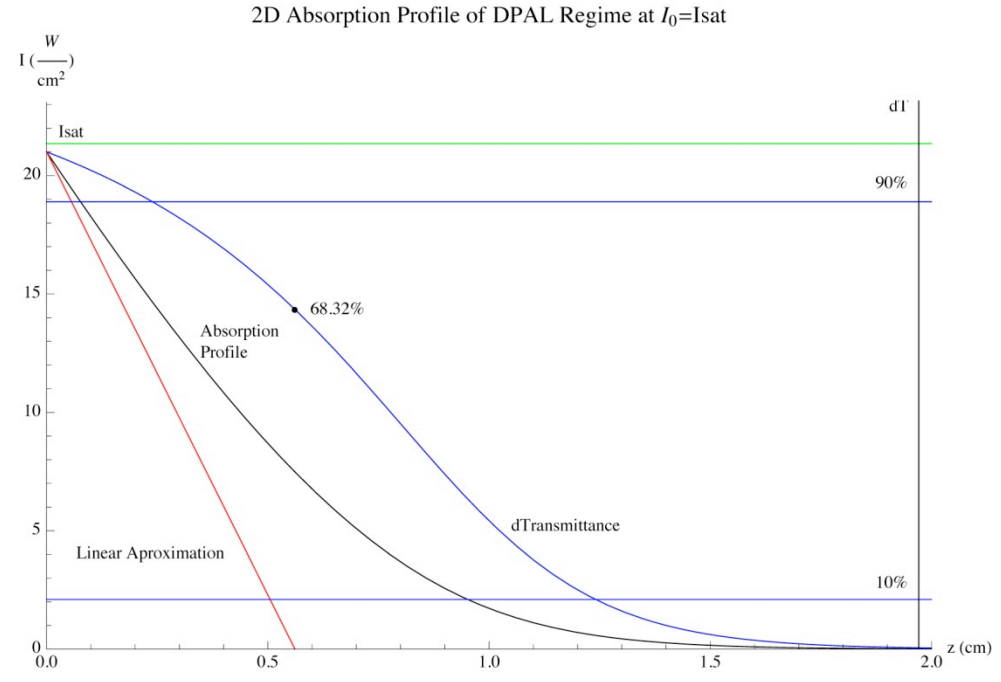

b.

Figure 29. Linear Approximation Performance at a.) 3xIsat and b.) Isat

The same single frequency analysis is done again, but this time with dTransmittance and linear approximation curves overlaid. A couple of bleached wave characteristics can be calculated from the model: distance at which dT equals 90%, distance at which it equals 10%, and the distance it takes for the wave to crash from 90% to 10% normalized to the ideal cell length. Also the value at which the linear approximation falls to zero as well as what is the dT value at this null length is tabulated in Table 13.

Table 14. Linear Approximation and dTransmittance Performance Numbers

Pump Intensity (x Isat)	LinearZnull	dT (znull)	90% (cm)	10% (cm)	90-10 (cm)	90-10 (Normalized)
1	0.56	68.32%	0.24	1.24	1.00	0.51
3	1.71	69.58%	1.04	2.56	1.52	0.51
5	2.86	71.17%	2.02	3.80	1.78	0.37
7	4.00	72.36%	3.07	5.01	1.94	0.33

As discussed before the linear approximation is a poor representation of the actual absorption profile at input pump intensities around Isat and a decent representation when intensities are way above Isat. The remarkable aspect of the linear approximation, however, lies in what it predicts the dTransmittance is. No matter what the input intensity is a good length to construct an absorbing cell is the distance predicted by z null. It appears that about 70 of 100 single photons will pass through without being absorbed. Another aspect that can be discerned is how hard the bleached wave crashes. The distance at which the differential transmittance decreases from 90% to 10% normalized to its cell length gives an indication for comparison. The lower this ratio is the more defined the bleached wave's front is. Visually this is seen in Figures 27a and 28b. The wave in 27a falls off dramatically where as the wave in 28b is more of a gentle slope.

Quasi Two Level Analytic Comparisons

Quasi Two Level Analytic Solution

An analytic solution to the rate equations and the differential law of absorption can be made if one assumes that the spin orbit relaxation between the $P_{3/2}$ and $P_{1/2}$ states is the fastest process compared to stimulation and emission. Essentially then the two states cannot be distinguished and the picture of the system becomes that of a quasi-two level absorption system. The two upper levels are statistically related by Boltzmann statistics as:

$$f = \frac{1}{1 + \frac{g_3}{g_2} \cdot Exp(-\Delta E_{32} / kT)} \tag{1.101}$$

As such the population of the statistically bound upper state becomes $n_2 = f n_U$ and $n_3 = (1-f)n_U$ and the ground state population is simply labeled n_L. Combined with the same constraint that the total population does not increase or decrease the rate equations for the quasi two level system become:

$$\begin{aligned}
\frac{dn_L}{dt} &= \frac{I_p}{h\nu_p}\sigma_{31} \cdot ((1-f)n_U - 2n_L) + \frac{(I_+ + I_-)}{h\nu_L}\sigma_{21}(f n_U - n_L) + \frac{n_U}{\tau} \\
\frac{dI_p}{dz} &= I_p \cdot \sigma_{31} \cdot ((1-f)n_U - 2n_L) \\
\frac{dI_+}{dz} &= \sigma_{21}(f n_U - n_L)\, I_+ \\
\frac{dI_-}{dz} &= -\sigma_{21}(f n_U - n_L)\, I_-
\end{aligned} \tag{1.102}$$

where τ is the effective lifetime of the combined upper states and I_+ and I_- are the right and left running intracavity laser intensities. A similar game can be played in which the rates in equation 1.104 are set to steady state conditions and from there the population inversion is calculated. This population inversion is then inserted into the differential law of absorption and what is obtained is a quasi two level description of pump absorption:

$$\frac{1}{I_p}\frac{dI_p}{dz} = -\sigma_{31}(\nu) n_{tot} \cdot \left(\frac{2 + \eta(3f-1)\cdot \frac{I_L(z)}{I_{sat}}}{1 + (3-f)\cdot \frac{I_p(z)}{I_{sat}} + \eta(f+1)\cdot \frac{I_L(z)}{I_{sat}}} \right) \qquad (1.103)$$

To compare with the rate equation analysis of this model the lasing intensity in equation 1.105 is set to zero and then the differential equation is solved for simply an absorbing case. Once accomplished the same analysis done for the rate equation analysis (REA) method is done for the quasi two level absorption analysis (QTLA) and the results compared. Figures 29 and 30 display both the absorption profile and differential transmittance profiles in space and in frequency:

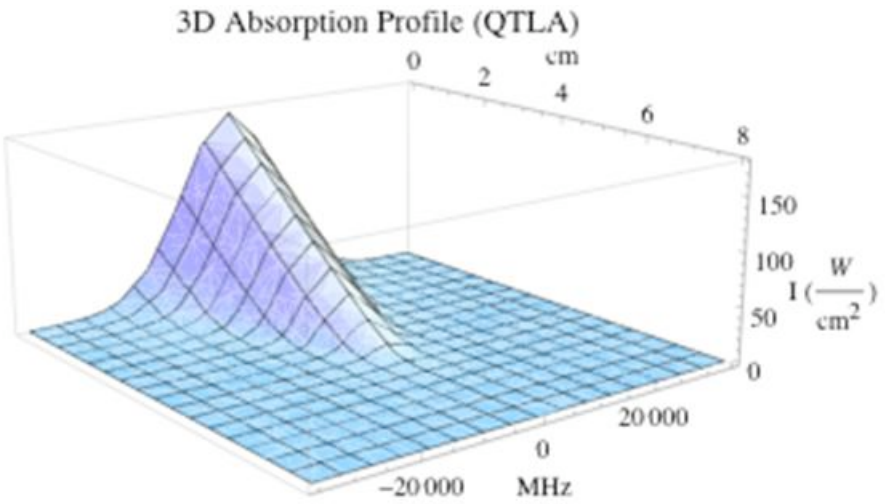

Figure 30. QTLA Profile

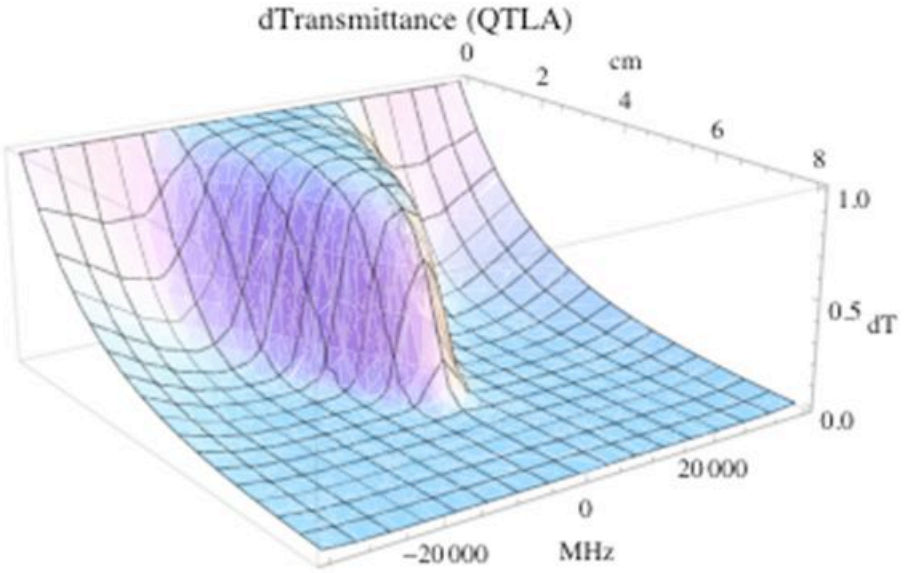

Figure 31. QTLA dTransmittance Profile

It is obvious that in comparison to Figures 21 and 25 the two solutions show similar features. Both exhibit a linear drop off in intensity and an exponential fall off as intensity nears zero. The bleached wave pictures look similar as well. Transparency of the cell crashing into an opaque curtain, however for the same parameters it appears that the bleached wave does not penetrate as far into the cell as in the rate equation analysis. To

further compare the two methods Figures 31-34 displays at different values of the saturation intensity the single frequency profile from the QTLA analysis versus the linear approximation of the rate equation analysis. Whereas the linear approximation undershot the REA curves it tends to be right on top of the QTLA curves. The following four figures show bleached wave characteristics and linear approximation performance values. Table 14 is augmented with these new performance values in Table 15 for ease of comparison.

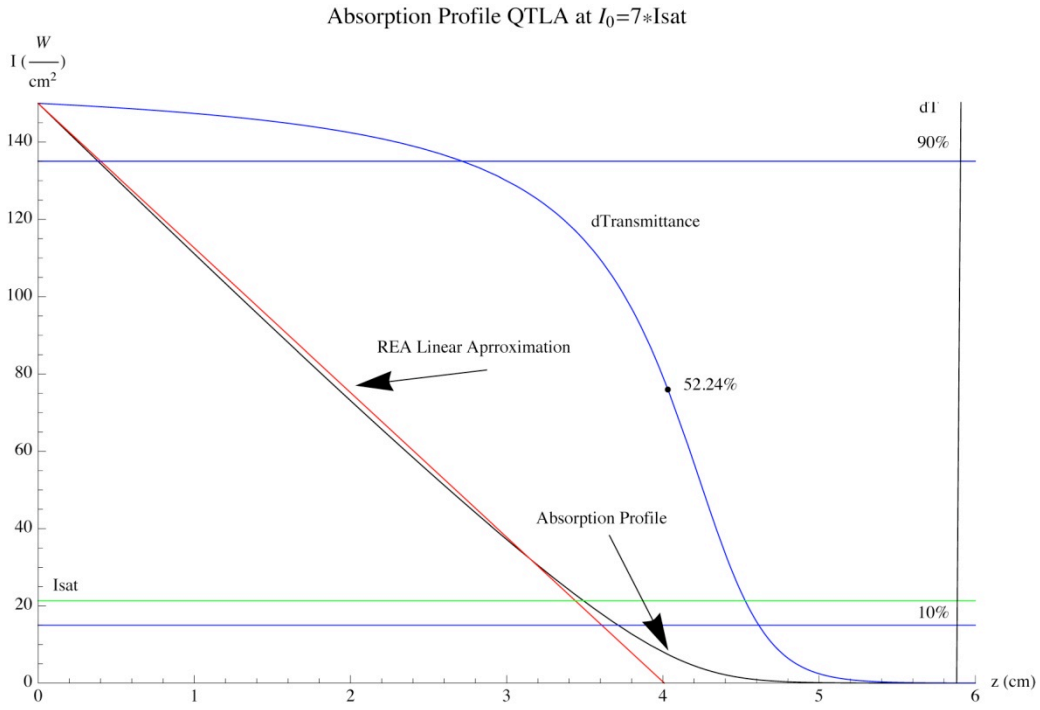

Figure 32. Linear Approximation Performance against QTLA at 7x Isat

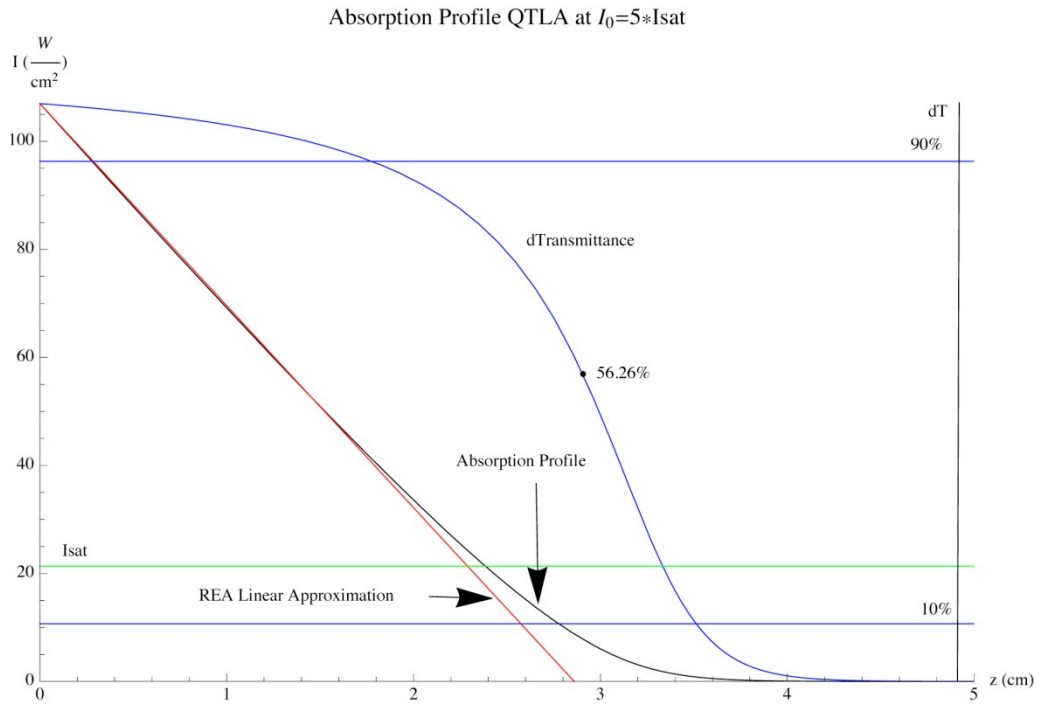

Figure 33. Linear Approximation Performance against QTLA at 5x Isat

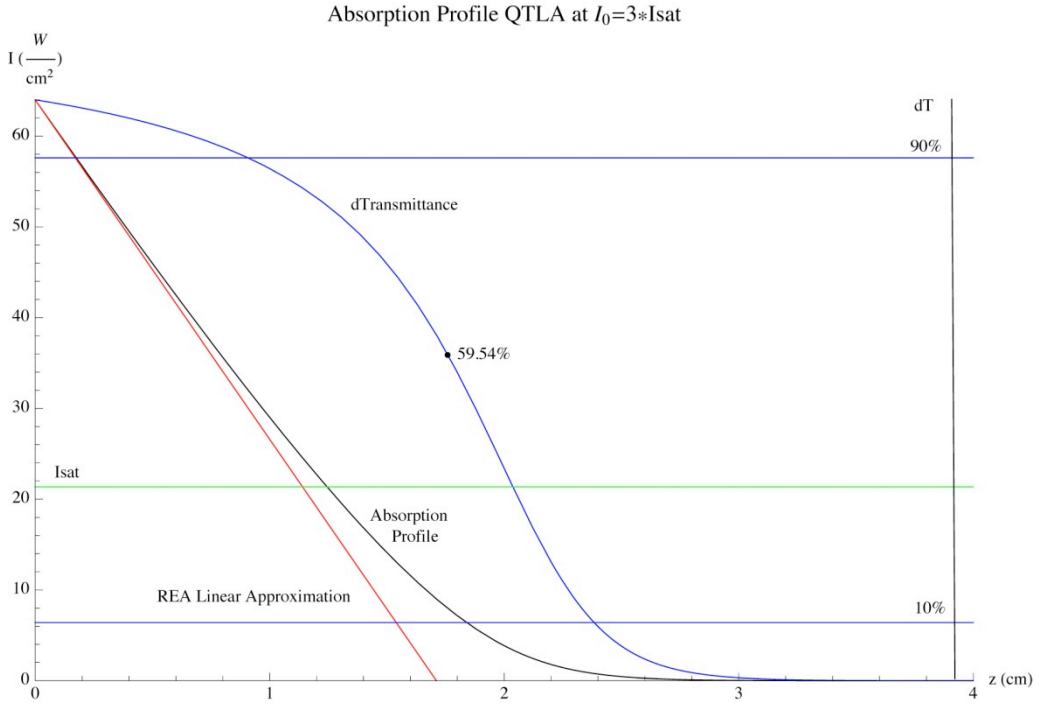

Figure 34. Linear Approximation Performance against QTLA at 3x Isat

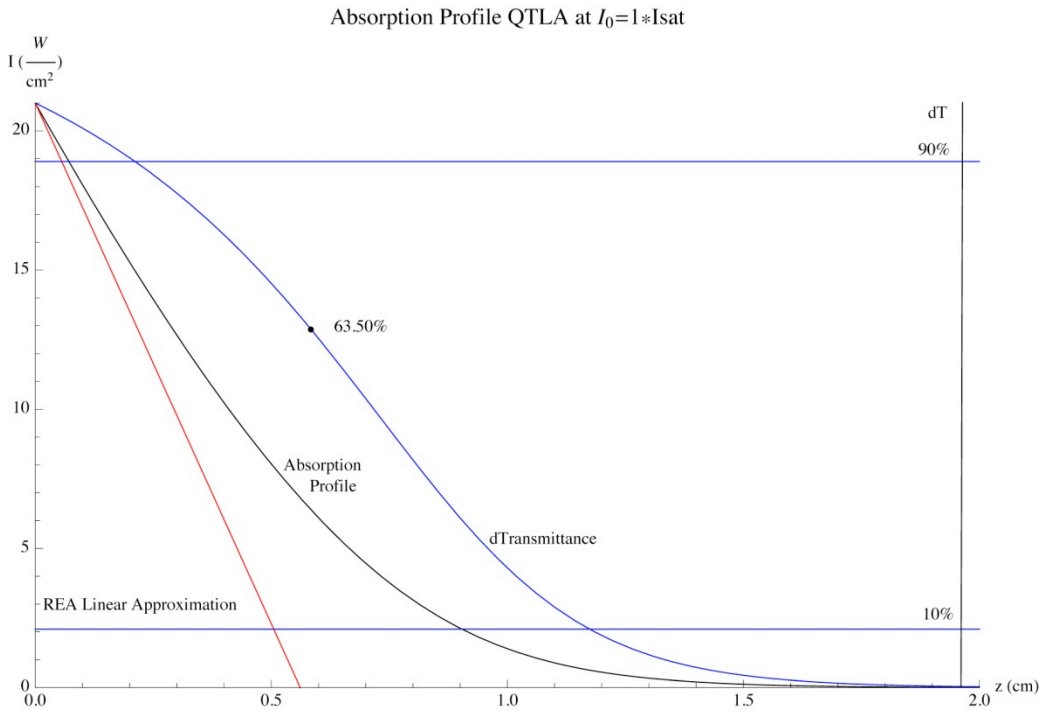

Figure 35. Linear Approximation Performance against QTLA at 1x Isat

Table 15. REA and QTLA Linear Approx dTransmittance Numbers

Pump Intensity (x Isat)	LinearZnull	dT (znull)	90% (cm)	10% (cm)	90-10 (cm)	90-10 (Normalized)
1	0.56	68.32%	0.24	1.24	1.00	0.51
3	1.71	69.58%	1.04	2.56	1.52	0.51
5	2.86	71.17%	2.02	3.80	1.78	0.37
7	4.00	72.36%	3.07	5.01	1.94	0.33
1	0.56	63.50%	0.21	1.17	0.97	0.49
3	1.71	59.54%	0.91	2.38	1.47	0.49
5	2.86	56.26%	1.78	3.51	1.73	0.41
7	4.00	52.24%	2.72	4.61	1.89	0.35

Quasi Two Level Absorption vs. Lasing

Once more we repeat the same type of analysis as done with the previous two sections using equation 1.105 with all processes active. The shape and function of the output laser intensity is highly dependent on the length of the cell. The QTL regime uses

a longitudinal geometry with key laser parameters being a function of cell length and the reflectivity of the output coupler. Also for lasing to take place a certain threshold must be crossed or else the laser will not run. The following quantities have been derived following the QTL approximation and derivation.

Effective Absorbance:

$$A = \frac{(3f-1)}{(f+1)}\sigma_{31}\cdot n_{tot}\cdot l_g - \frac{(3-f)}{(f+1)}\cdot\frac{\sigma_{31}}{\sigma_{21}}\cdot Ln\left[\frac{1}{\sqrt{r}}\right] \tag{1.104}$$

where l_g is the cell length and r is the output coupling parameter.

Laser Threshold Intensity:

$$I_{th} = \frac{I_{sat}}{(1-e^{-A})(1+f)}\cdot\left\{\left(\frac{\sigma_{31}}{\sigma_{21}}\right)Ln\left[\frac{1}{\sqrt{r}}\right] + \sigma_{31}\cdot n_{tot}\cdot l_g\right\} \tag{1.105}$$

Slope Efficiency:

$$\eta_{slope} = \left(\frac{\nu_p}{\nu_L}\right)(1-e^{-A}) \tag{1.106}$$

Output Laser Intensity:

$$I_{out} = \eta_{slope}(I_p(0) - I_{th}) \tag{1.107}$$

In order to setup a lasing scenario first a 2 cm cell was chosen and the an input power was picked, 70 W/cm^2, such that the cell was nearly completely bleached. The output coupling constant was chosen to be 0.5. The rest of the system parameters were identical to the DPAL regime parameters. Based on the system parameters the following were established for lasing threshold as well as the laser output power in frequency space.

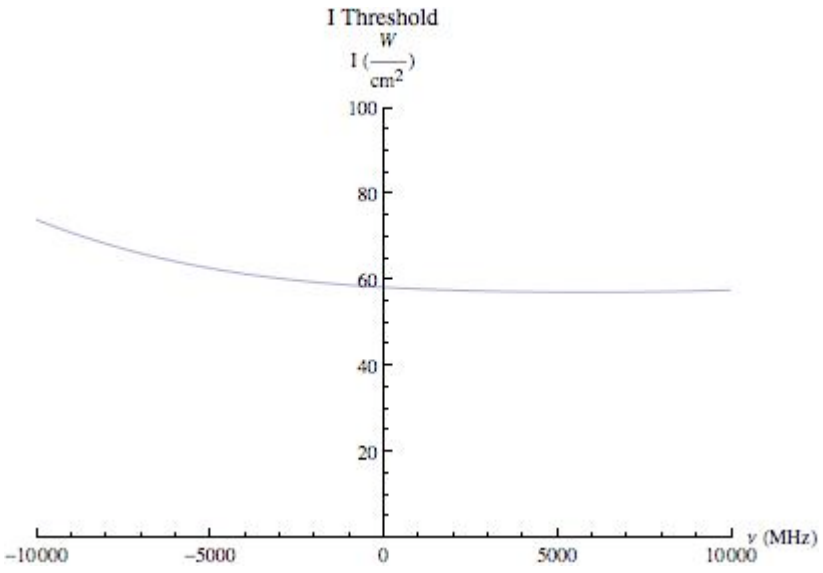

Figure 36. I Threshold

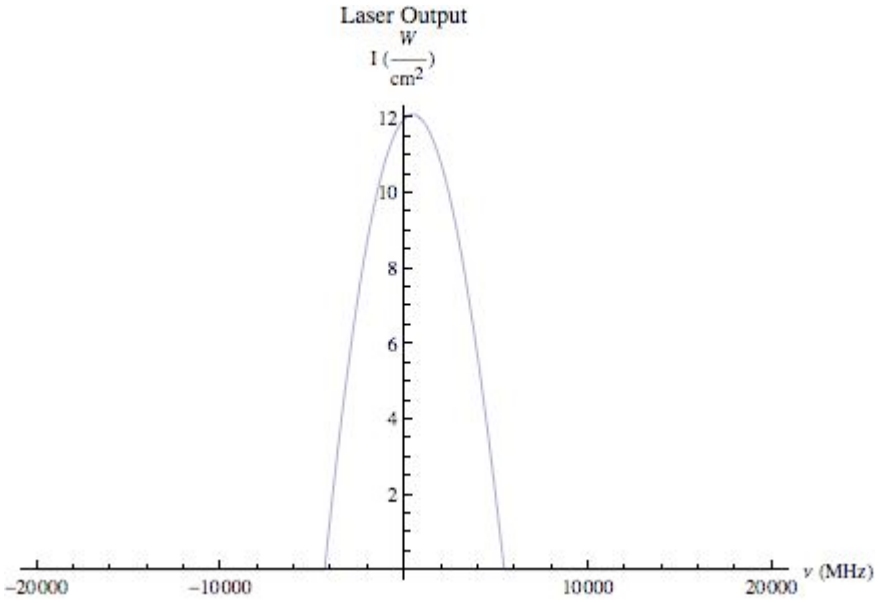

Figure 37. Laser Output

By examining equation 1.105 it's obvious that any difference between the absorption profile with and without lasing will occur between -4000 and 5800 MHz from inspecting Figure 35. Equation 1.109 explains that above threshold the output intensity varies linearly with respect to the input pump intensity. Taking these facts into consideration we look at the absorption profiles of both cases at zero frequency for the following input intensities: 56 (threshold), 70, 140, and 210 W/cm^2.

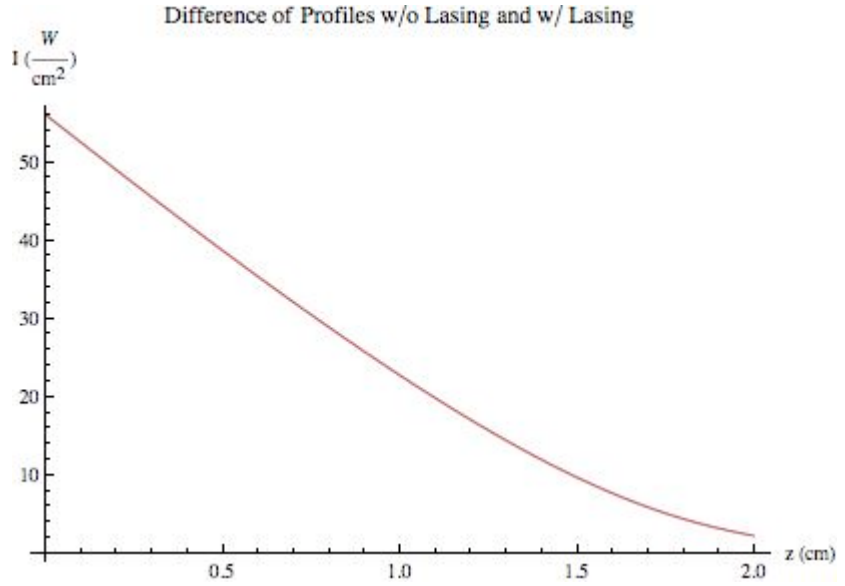

Figure 38. Difference of Profiles w/o Lasing and w/ Lasing at I_0=56

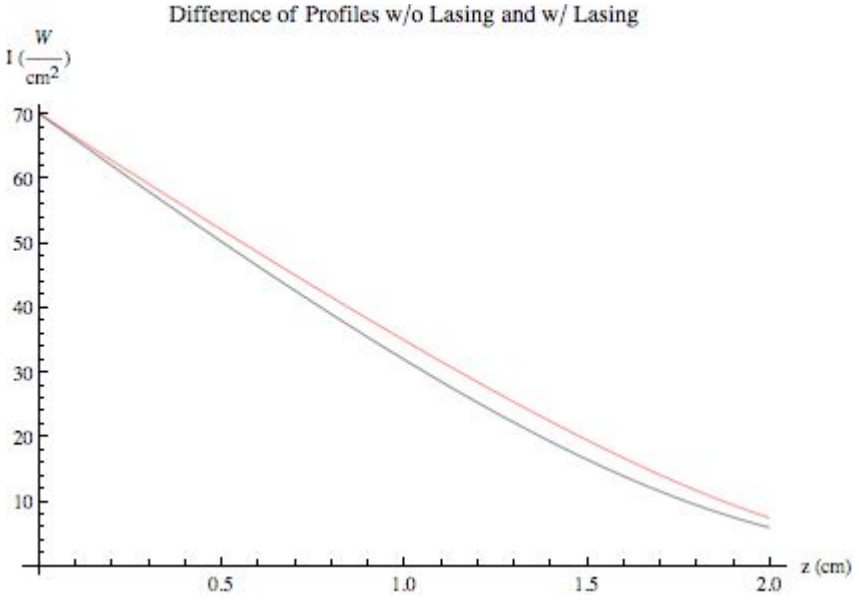

Figure 39. Difference of Profiles w/o Lasing and w/ Lasing at I_0=70

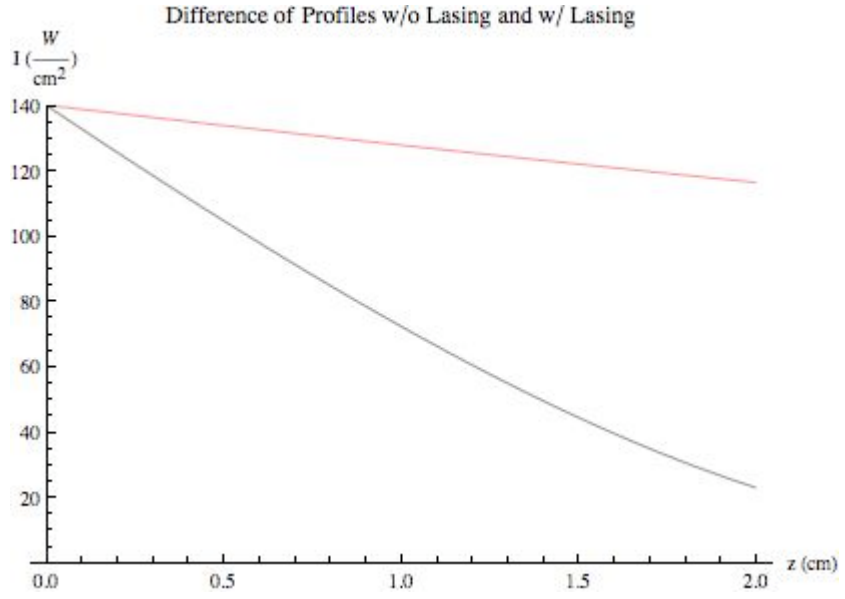

Figure 40. Difference of Profiles w/o Lasing and w/ Lasing at I_0=140

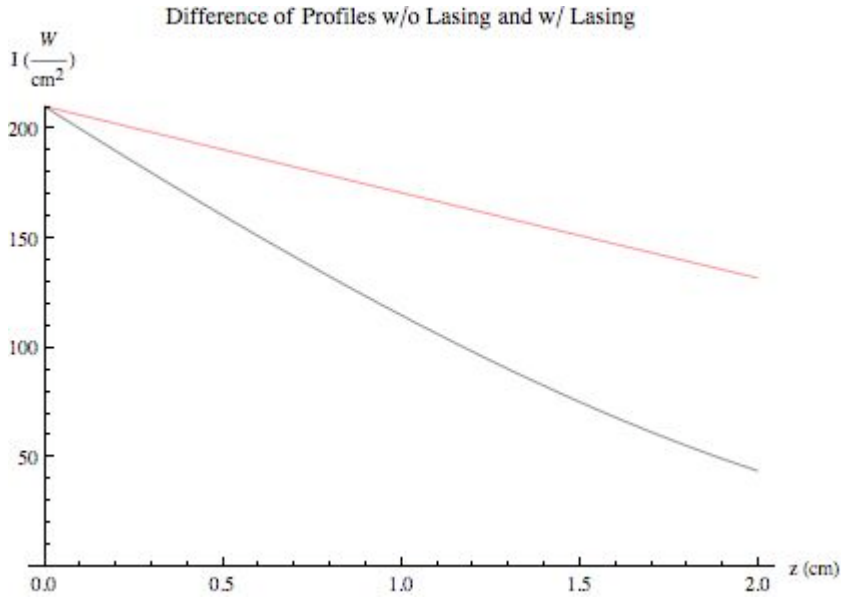

Figure 41. Difference of Profiles w/o Lasing and w/ Lasing at I_0=210

Figure 37 shows no marked difference in absorption profiles. This of course makes perfect sense because the input intensity is at the required threshold for lasing. Figures 38-40 however have the necessary intensity to achieve lasing. A remarkable result occurs: no matter the input power above threshold the lasing condition seems to keep absorption profile fairly constant. The top curves of Figures 38-40 represent the absorption profile without lasing. We can see the key feature of linearity when the input intensity is significantly above Isat however the lasing prevents this limit from being achieved. This implies an important aspect about cell size and lasing. For a given set of parameters the calculated intensity for lasing threshold must at minimum be able to bleach the entire cell length. If this is achieved Figure 38-40 imply that this bleach length will remain constant no matter how high above threshold the input intensity is.

IV. Conclusions

Simulation Scenarios

Beer's Law Regime

The outputs of this model to the Beer's Law regime were expected since the differential law of absorption has an analytical solution when the input intensity is well below saturation intensity. As shown in Figure 20 however with the rapid absorption along the hyperfine peaks a transmission window is created which could be useful for optical systems. The advantages of such a system is first the bandwidth of the window is controlled through increasing or decreasing the system pressure. As such the window becomes a user controlled variable. Second since all alkali metals have similar atomic structure, mainly the doublet absorption cross section, different center frequencies can be chosen by using a different alkali metal. As such one could engineer a variable bandwidth transmission window whose center frequencies are those of each alkali metals unique fine structure transition frequency.

It is also not too surprising that the dTransmittance profile looks very similar to the absorption profile. The analytic solution to Beer's Law when solved and the derivative taken with respect to the input intensity I_0 simply yields another exponential. The advantage of the Beer's Law simplicity lends itself to be an easy benchmark to test any absorbing model. The rate equation analysis that this model used made no such Beer's Law approximation, however it is expected that when Beer's Law conditions hold the full solution should yield the analytic Beer's Law solution. It is obvious from Figures 20, 23, and 24 that the rate equation analysis yields what is expected. All rate equation

solutions derived or modeled should always be first tested under Beer's Law conditions since it is such an easy benchmark of performance.

DPAL Regime

The DPAL regime took a look at the other end of the spectrum: high system pressure and high input intensity. No such doublet absorption was observed since the hyperfine peaks were pressure broadened into one peak. By far pressure has the most variable effects on lineshape broadening. Natural broadening has little to no effect in when compared to Doppler and pressure broadening. Even Doppler broadening has its limitations because the only way to broaden the lineshape is to increase temperature and if the temperature is continually raised eventually one might start melting parts of their apparatus. Not to mention raising system temperature for the purposes of broadening a lineshape could introduce thermal regulation issues that are not accounted for in this model. When needed pressure should always be the chief mechanism to broaden any lineshape in such an absorbing configuration.

Upon solving the differential law of absorption using the population densities derived from the rate equations while the input power was above Isat proved to have no analytical solution. In fact the numerical solution involves a function called the Product Log, or the Lambert-W function, which is an inherently complex function. So even when modeling this solution one needs to understand that do to its complex nature multiple solutions exist. Finding the right solution that models real world experiment, if they exist, could prove to be a significant task for different developments of rate equations.

In the upper limit that the input intensity was significantly higher than Isat an approximation to the differential law of absorption was made which turned out to be

analytic. That solution was the linear approximation. How high the input has to be above Isat where the linear approximation becomes an accurate account of the absorption profile simply has to be determined experimentally. From Figure 22 the actual profile is undoubtedly a mix of linear and exponential character. Even at an input intensity of 7x Isat the exponential quality of the solution takes hold rather quickly. Determining where the transition from linear to exponential character occurs is nearly impossible to tell.

Once the solution to the saturation law using the rate equation analysis was numerically solved taking the derivative of this solution with respect to the input intensity led to a new quantity termed differential transmittance. The differential transmittance is a representation for the bleached wave. The wave front of the bleached wave marks where the region of transparency ends and where an opaque region begins. In practice an actual system would need, for optimal performance, the cell length to match the length of the bleached wave. Any cell length longer than this wave will lead to a hit in absorption performance which will directly degrade the laser output performance.

The null distance predicted by the linear approximation while poor for predicting where the input is attenuated to zero gave a pretty consistent dTransmittance prediction regardless if the system was in a Beer's Law or DPAL regime. Table 14 shows that if the linear approximation is used to make a first estimate on cell length, about 70% of single photons will bleach through the cell. Since the linear approximation has such a simple form, equation 1.102, if one knows beforehand what system parameter they want to run, lifetimes, and kinetic constants, equation 1.102 simply needs to be inverted and the predicted cell length will be a very good estimate to run an absorbing system. Looking at the slope of equation 1.102,

$$m = -\frac{2 \cdot N \cdot z \cdot Isat(\upsilon) \cdot \sigma(\upsilon) \cdot (1 - k_{23} k_{32} \tau_2 \tau_3)}{(3 + k_{32} \tau_2) A_{31} \tau_3} \tag{1.108}$$

it is obvious that what a DPAL system is most sensitive to is the concentration of alkali. Barring that any further variations due to pressure and temperature will be contained in how much lifetimes and the saturation intensity vary. Nonetheless the linear approximation is concluded to be a good starting point in creating a DPAL absorbing cell.

Comparison to Quasi Two Level Analysis

To effectively compare the rate equation model with the quasi two level model we take a look at how the population inversion density changes with initial input pressure at particular choices of system pressure. The population inversions of the REA model and the QTL model are

$$\frac{N_3 - N_1}{N} = \frac{-2(1 - k_{32} k_{23} \tau_2 \tau_3)}{(1 - k_{32} k_{23} \tau_2 \tau_3) + \frac{I}{Isat}(3 + 2k_{32} \tau_2) A_{21} \tau_3} \tag{1.109}$$

$$\frac{N_3 - N_1}{N} = \frac{-2}{1 + (3 - f)\frac{I}{Isat}} \tag{1.110}$$

respectively. When there is no pump present both of these normalized inversions will evaluate to negative two and as the pump goes to infinity these values will evaluate to

zero. The quasi two level model assume beforehand that the second and third levels coupled. This statement in the REA model amounts to a very high system pressure for this would force the mixing rate to be the fastest rate in the system.

Figure 41 displays a set of these curves for different total system pressures. At any particular input power we see that it is harder to maintain a N3, N1 population inversion. For instance at an initial pump intensity of 500 W/cm^2 at a system pressure of 400 torr (curve A) the value of the inversion is close to zero or in other words the population in the first and third states are comparable. However looking at curve E, where the system is at 20000 torr, we find more population in the first state than the third state. The reasoning behind this is that at high system pressures the mixing rate from state 3 to state 2 is faster than the pumping rate; state three is being de-populated and it is harder to maintain the N3, N1 inversion.

For a particular pressure when the normalized population inversions are compared between the two models we expect the quasi two level inversion to be slightly harder to maintain than that of the REA model. Figure 42 shows the two models compared at system pressures of 400, 6000, and 20000 torr. In each case the QTL inversion maintains a slight edge in depopulating its third level to the second level. In each case the REA normalized population inversion approaches that of the QTL, but never surpasses it. This shows that as system pressure is increased the REA model will predict pump attenuations closer to that of the QTL because the attenuation depends on the N3, N1 population inversion. The REA model converges to the QTL model under QTL assumptions.

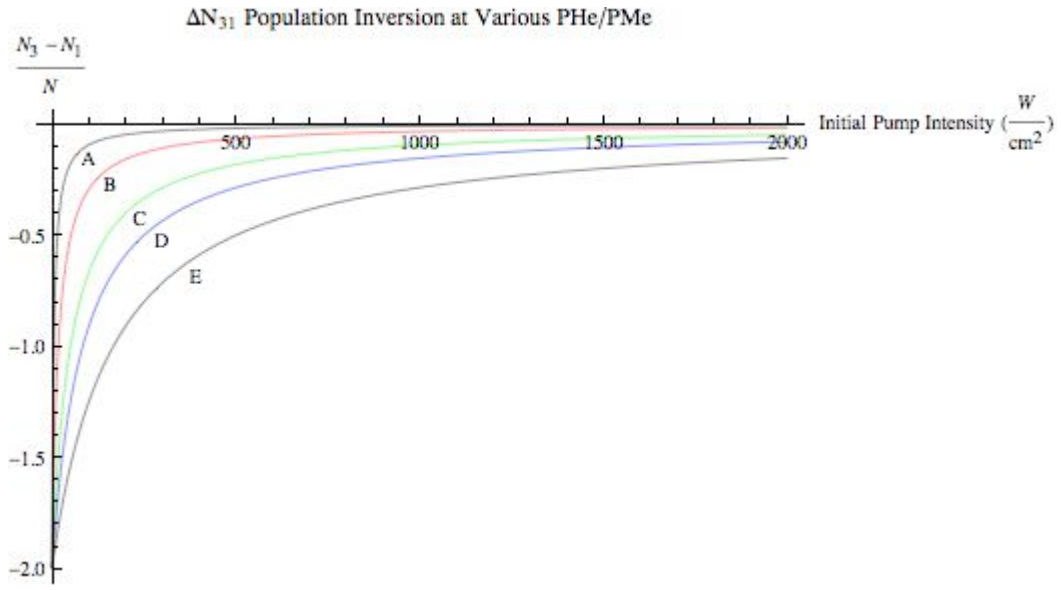

Figure 42. Normalized Population Inversions at various system pressures. Curve A: 400 torr; Curve B: 2000 torr; Curve C: 6000; Curve D: 10000; Curve E: 20000

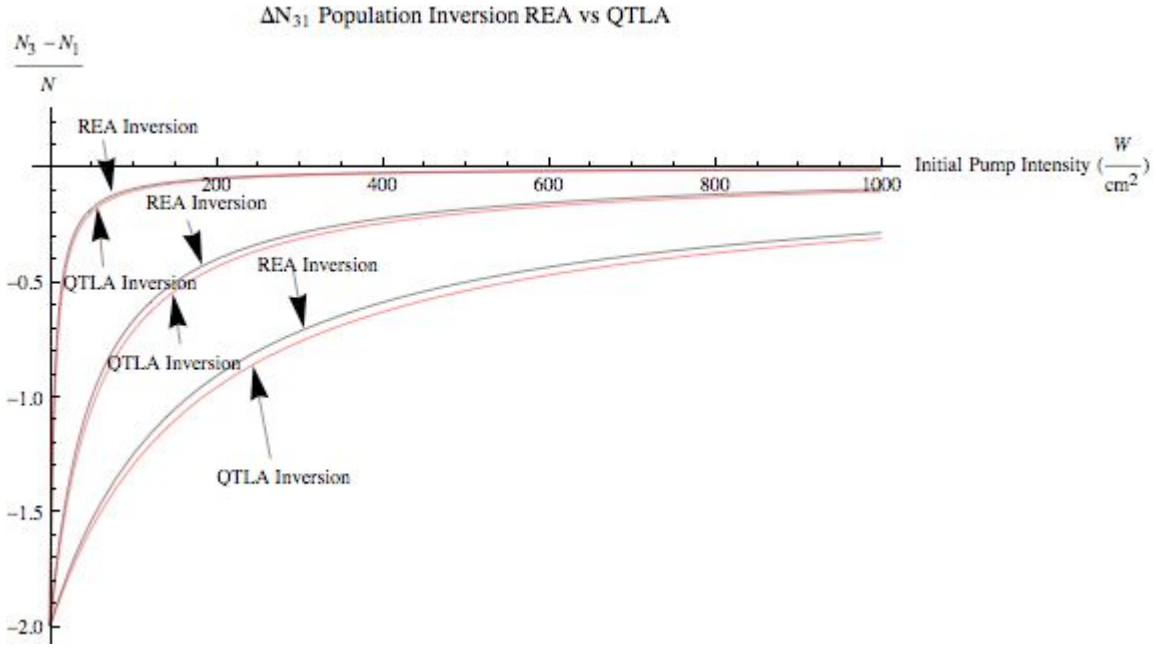

Figure 43. Normalized Population Inversions of REA model vs QTLA model at system pressure of 400, 6000, and 20000 torr.

Comparison of QTL Absorption and Lasing

The final analysis of this paper was to compare the absorption profiles within the QTL analysis between lasing off and lasing on. The laser parameters, effective absorbance, slope efficiency, and threshold were all solely defined around system parameters with the value of the output coupler reflectivity user defined. A test scenario was the set up in which a 2 cm cell was chosen and the system parameters the same as the DPAL regime. Figures 36 display such a comparison. As seen in Figure 37 the initial input intensity was at threshold so no lasing effects occurred and that is why only one profile exists. The pictures differ drastically in Figures 38-40. The upper curves, which represent no lasing, simply blast through the cell. However the curves when lasing is running are nearly constant regardless of what the input power is. In fact they look really similar to the profile where the input intensity is at laser threshold.

To make sense of this phenomenon the quasi two level system essentially is describing a photon engine. A photon absorbs energy from the pump, is excited to the second level, and then returns to the ground state by stimulated emission. This process happens over and over again hence the photon engine moniker. With this repeated process pump intensity must be devoted to those photons that have run this cycle repeatedly. This is why the absorption profiles with lasing on in Figures 38-40 remain nearly the same. The reason why they are not the same as the ideal profile in figure 37 is because quantum and slope efficiencies will never be 100%. The further the laser quantum efficiency deviates from 100% the less likely the absorption profile will mimic the ideal profile in which the input intensity is threshold intensity. This discovery leads to another engineering benchmark. The laser threshold value, computed from system

parameters, must be able to entirely bleach the selected cell length. If this is not the case then adequate absorption cannot take place and the laser will not run.

Combining this result with the linear approximation for a quasi two level system we have a benchmark:

$$I(\nu) \simeq I_{Threshold}(z_0) - \frac{z_0 \cdot N \cdot I_{sat} \cdot \sigma_{31} \cdot 2}{3 - f} \tag{1.111}$$

Once a desired cell length is chosen, z_0, and inserted into equation 1.113, if the resultant answer is less than or equal to zero and the threshold is much higher than the saturation frequency, so that the linear approximation is fairly accurate, the laser will not run.

Recommendations for Future Modeling Work

The next step for this model to take would be to implement lasing from a Rate Equation Analysis standpoint. This would involve deriving additional rate equations that account for the photons being created along the lasing D1 manifold as the spin orbit processes regulate population from the D2 to D1 manifold. Solving the equations would be a mere exercise in Mathematica modeling skill, but inherent in the lasing rate equations will be the next big problem for this model to solve: what are the ideal geometrical configurations that would maximize laser output? One could vary the cell from a longitudinally pumped cell to a transversely pumped cell. Or perhaps the cell could be longitudinally pumped but lase transversely? The size and shape of the cavity would force different cavity modes to be explored and analyzed and the configurations are practically limitless. So by establishing two to three different geometrical

configurations and then solving pump rates and lasing rates a stronger engineering hold of what a DPAL system should look like will come more to light.

Recommendations for Future Experimental Work

The robustness of this model must be tested against a wide range of scenarios. Two particular experiments can test this model right away. The first experiment would be absorption along a longitudinal axis of an absorbing cell. Multiple test scenarios should be run at a wide variety of temperatures, pressures, input powers, and varying compositions of foreign species especially those scenarios that lead to a bleached wave being formed. This way profiles can be compared readily to those outputted by this model.

A second experiment can be devised to test the bleached wave and linear approximation. First, bleaching conditions should be established based of a cell length predicted by the linear approximation. Second, once bleaching conditions are established a secondary pump slight detuned from the primary pump can be used at low power to inject photons into the system that would not affect the primary input pump power. If these low power photons can be detected on the output end of the cell an experimental picture of the bleached wave can be detected and then compared to the theoretical dTransmission value predicted from the linear approximation. Then system parameters can be slightly adjusted such that the bleached wave creeps back into the cell or completely blasts through the length. The same low power photons can be injected to see if the distance of the bleached wave changes as predicted by this model.

Appendix A

Development of Population Inversion

Rate Equations for a three level system:

$$\frac{dN_3}{dt} = N_3\left(\frac{-I_P(\nu)\sigma_{31}}{h\nu_P} - \frac{1}{\tau_3}\right) + N_2 k_{23} + N_1\left(\frac{I_P(\nu)\sigma_{31}}{h\nu_P}\frac{g_3}{g_1} + k_{13}\right) \tag{2.1}$$

$$\frac{dN_2}{dt} = N_3 k_{32} + N_2\left(\frac{-I_L(\nu)\sigma_{21}}{h\nu_L} - \frac{1}{\tau_2}\right) + N_1\left(\frac{I_L(\nu)\sigma_{21}}{h\nu_L}\frac{g_2}{g_1} + k_{12}\right) \tag{2.2}$$

$$\frac{dN_1}{dt} = -\left(\frac{dN_2}{dt} + \frac{dN_3}{dt}\right) \tag{2.3}$$

Substitute the total number of alkali atoms, $N_2 = N - N_1 - N_3$, into equation 2.1.

$$\frac{dN_3}{dt} = N_3\left(\frac{-I_P(\nu)\sigma_{31}}{h\nu_P} - \frac{1}{\tau_3} - k_{23}\right) + (0)N_2 + N_1\left(\frac{I_P(\nu)\sigma_{31}}{h\nu_P}\frac{g_3}{g_1} + k_{13} - k_{23}\right) + Nk_{23} \tag{2.4}$$

Set all time derivatives to zero for steady state conditions and rearrange equations 2.2, 2.3, and 2.4 into a matrix equation:

$$\begin{pmatrix} \left(\frac{-I_P(\nu)\sigma_{31}}{h\nu_P} - \frac{1}{\tau_3} - k_{23}\right) & 0 & \left(\frac{I_P(\nu)\sigma_{31}}{h\nu_P}\frac{g_3}{g_1} + k_{13} - k_{23}\right) \\ k_{32} & \left(\frac{-I_L(\nu)\sigma_{21}}{h\nu_L} - \frac{1}{\tau_2}\right) & \left(\frac{I_L(\nu)\sigma_{21}}{h\nu_L}\frac{g_2}{g_1} + k_{12}\right) \\ \left(\frac{I_P(\nu)\sigma_{31}}{h\nu_P} + \frac{1}{\tau_3} - k_{32}\right) & \left(\frac{I_L(\nu)\sigma_{21}}{h\nu_L} + \frac{1}{\tau_2} - k_{23}\right) & \left(\frac{-I_P(\nu)\sigma_{31}}{h\nu_P}\frac{g_3}{g_1} - k_{13} - k_{12} - \frac{I_L(\nu)\sigma_{21}}{h\nu_L}\frac{g_2}{g_1}\right) \end{pmatrix} \begin{pmatrix} N_3 \\ N_2 \\ N_1 \end{pmatrix} = \begin{pmatrix} -N_3 k_{23} \\ 0 \\ 0 \end{pmatrix} \tag{2.5}$$

Multiply both sides by $A_{21}A_{31}$ in order to get equation 2.3 in terms of saturation intensities. Use Kramer's Rule for a 3x3 matrix to solve for N_3, N_2, and N_1.

$$S_3 = \begin{pmatrix} -N_3 k_{23} A_{21} A_{31} & 0 & \left(\frac{I_P(\nu)A_{21}}{I_{SP}}\frac{g_3}{g_1} + (k_{13}-k_{23})A_{21}A_{31}\right) \\ 0 & \left(\frac{-I_L(\nu)A_{31}}{I_{SL}} - \frac{A_{21}A_{31}}{\tau_2}\right) & \left(\frac{I_L(\nu)A_{31}}{I_{SL}}\frac{g_2}{g_1} + k_{12}A_{21}A_{31}\right) \\ 0 & \left(\frac{I_L(\nu)A_{31}}{I_{SL}} + \frac{A_{21}A_{31}}{\tau_2} - k_{23}A_{21}A_{31}\right) & \left(\frac{-I_P(\nu)A_{21}}{I_{SP}}\frac{g_3}{g_1} - (k_{13}+k_{12})A_{21}A_{31} - \frac{I_L(\nu)A_{31}}{I_{SL}}\frac{g_2}{g_1}\right) \end{pmatrix} \quad (2.6)$$

$$S_2 = \begin{pmatrix} \left(\frac{-I_P(\nu)A_{21}}{I_{SP}} - \frac{A_{21}A_{31}}{\tau_3} - k_{23}A_{21}A_{31}\right) & -N_3 k_{23} A_{21} A_{31} & \left(\frac{I_P(\nu)A_{21}}{I_{SP}}\frac{g_3}{g_1} + (k_{13}-k_{23})A_{21}A_{31}\right) \\ k_{32}A_{21}A_{31} & 0 & \left(\frac{I_L(\nu)A_{31}}{I_{SL}}\frac{g_2}{g_1} + k_{12}A_{21}A_{31}\right) \\ \left(\frac{I_P(\nu)A_{21}}{I_{SP}} + \frac{A_{21}A_{31}}{\tau_3} - k_{32}A_{21}A_{31}\right) & 0 & \left(\frac{-I_P(\nu)A_{21}}{I_{SP}}\frac{g_3}{g_1} - (k_{13}+k_{12})A_{21}A_{31} - \frac{I_L(\nu)A_{31}}{I_{SL}}\frac{g_2}{g_1}\right) \end{pmatrix} \quad (2.7)$$

$$S_1 = \begin{pmatrix} \left(\frac{-I_P(\nu)A_{21}}{I_{SP}} - \frac{A_{21}A_{31}}{\tau_3} - k_{23}A_{21}A_{31}\right) & 0 & -N_3 k_{23} A_{21} A_{31} \\ k_{32}A_{21}A_{31} & \left(\frac{-I_L(\nu)A_{31}}{I_{SL}} - \frac{A_{21}A_{31}}{\tau_2}\right) & 0 \\ \left(\frac{I_P(\nu)A_{21}}{I_{SP}} + \frac{A_{21}A_{31}}{\tau_3} - k_{32}A_{21}A_{31}\right) & \left(\frac{I_L(\nu)A_{31}}{I_{SL}} + \frac{A_{21}A_{31}}{\tau_2} - k_{23}A_{21}A_{31}\right) & 0 \end{pmatrix} \quad (2.8)$$

The solution to each component becomes:

$$N_3 = \frac{Det[S_3]}{Det[S]}$$
$$N_2 = \frac{Det[S_2]}{Det[S]} \qquad (2.9)$$
$$N_1 = \frac{Det[S_1]}{Det[S]}$$

The population inversion, $N_3 - \frac{g_3}{g_1} N$, becomes, with lasing set to $I_L = 0$, equation 2.10 below:

$$\frac{N(-2 + k_{13}\tau_3 + k_{23}k_{12}\tau_2\tau_3 + 2k_{32}k_{23}\tau_2\tau_3)}{(1 + k_{12}\tau_2 + (k_{13} + k_{23}(k_{12} - k_{32})\tau_2 + k_{13}k_{32}\tau_2)\tau_3) + \frac{I}{I_{SP}}(3 + k_{12}\tau_2 + 2k_{32}\tau_2)A_{21}\tau_3} \qquad (2.10)$$

Bibliography

Demtroder, Wolfgang. *Laser Spectroscopy: Basic Concepts and Instrumentation.* Berlin: Springer-Verlag, 2003.

Gross, Kevin C. Class notes, PHYS 661, Atomic and Molecular Spectroscopy. Department of Engineering Physics, Air Force Institute of Technology, Wright-Paterson AFB OH, Winter Quarter 2008.

Hager, Gordon D. and others. "A Quasi-Two Level Analytic Model for End Pumped Alkali Metal Vapor Lasers". Department of Engineering Physics, Air Force Institute of Technology, Wright-Patterson Air Force Base, OH. (Draft May 2008).

Hilborn, Robert C. "Einstein coefficients, cross section, f values, dipole moments, and all that," *Am. J. Phys.*, 50: 982-986 (1982). (Revised February, 2002).

Konefal Z., "Observation of collision induced processes in rubidium-ethane vapour," *Optics Communication*, 164:95-105 (1999).

Krause, L., "Collisional Excitation Transger Between the $^2P_{1/2}$ and $^2P_{3/2}$ Levels in Alkali Atoms," *Applied Optics*, Vol. 5, No. 9: 1375-1382 (Sep 1966).

Shankar, Ramamurti. *Principles of Quantum Mechanics Second Edition*. New York: Plenum Press, 1994.

Steck, Daniel A, "Cesium D Line Data," available online at http://steck.us.alkalidata (revision 2.1, September 2008).

Steck, Daniel A, "Rubidium 85 D Line Data," available online at http://steck.us.alkalidata (revision 0.2, 1 September 2008).

Steck, Daniel A, "Rubidium 87 D Line Data," available online at http://steck.us.alkalidata (revision 2.1, 1 September 2008).

Verdyne, Joseph T. *Laser Electronics Second Edition*. Englewood Cliffs, New Jersey: Prentics-Hall, 1981

REPORT DOCUMENTATION PAGE

Form Approved
OMB No. 074-0188

1. REPORT DATE *(DD-MM-YYYY)*	2. REPORT TYPE	3. DATES COVERED *(From – To)*
27-03-2009	Master's Thesis	March 2008 – March 2009

4. TITLE AND SUBTITLE

Theoretical Model Analysis of Absorption of a Three level Diode Pumped Alkali Laser

5a. CONTRACT NUMBER

5b. GRANT NUMBER

5c. PROGRAM ELEMENT NUMBER

6. AUTHOR(S)

Lewis II, Charlton D., 1st LT, USAF

5d. PROJECT NUMBER

5e. TASK NUMBER

5f. WORK UNIT NUMBER

7. PERFORMING ORGANIZATION NAMES(S) AND ADDRESS(S)

Air Force Institute of Technology
Graduate School of Engineering and Management (AFIT/EN)
2950 Hobson Way, Building 640
WPAFB OH 45433-8865

8. PERFORMING ORGANIZATION REPORT NUMBER

AFIT/GAP/ENP/09-M07

9. SPONSORING/MONITORING AGENCY NAME(S) AND ADDRESS(ES)

High Energy Laser Joint Task Office
901 University Blvd SE, Suite 100
Albuquerque, NM 87106
Ackerman, Harro (505)248-8108

10. SPONSOR/MONITOR'S ACRONYM(S)
HEL-JTO

11. SPONSOR/MONITOR'S REPORT NUMBER(S)

12. DISTRIBUTION/AVAILABILITY STATEMENT

APPROVED FOR PUBLIC RELEASE; DISTRIBUTION UNLIMITED.

13. SUPPLEMENTARY NOTES

14. ABSTRACT

This paper models the absorption phenomena of light in a three level diode pumped alkali laser system. Specifically this model calculates for a user defined set of system parameters the attenuation of the input pump beam and characteristics of the bleached wave. Using Wolfram's Mathematica 6.0 software all necessary physics for an accurate description of absorption was modeled from first principles: energy levels, cross sections, spin-orbit kinetic processes, saturation frequencies, pump attenuation, and differential transmittance, which is a representation of the bleached wave. A specific DPAL scenario was simulated, 455K system temperature, alkali concentration of $6.1 \cdot 10^{13}$, and a system pressure of 200 torr of He and 600 torr of Ethane. For a range of initial input intensities the linear approximation to the beam attenuation predicted consistently a differential transmittance value of 70%. It was concluded that the linear approximation is a good indicator of the distance a bleached wave penetrates an absorbing cell. This model was also benched marked against the quasi two level model. In the limit of high system pressure the simulated model converged to the same population inversion as that of the quasi two level regime. Finally, within the quasi two level regime a closed analytic equation was developed to describe under what conditions the system would lase.

15. SUBJECT TERMS

DPAL, Bleached Wave, Gas/Electric Laser

16. SECURITY CLASSIFICATION OF:			17. LIMITATION OF ABSTRACT	18. NUMBER OF PAGES	19a. NAME OF RESPONSIBLE PERSON
a. REPORT	b. ABSTRACT	c. THIS PAGE			Glen P. Perram, PhD
U	U	U	UU	115	19b. TELEPHONE NUMBER *(Include area code)* (937) 785-3636 x4504 (glen.perram@afit.edu)